Article

The Loss of PPARγ Expression and Signaling Is a Key Feature of Cutaneous Actinic Disease and Squamous Cell Carcinoma: Association with Tumor Stromal Inflammation

Raymond L. Konger [1,2,*] , Xiaoling Xuei [3], Ethel Derr-Yellin [2], Fang Fang [3], Hongyu Gao [3] and Yunlong Liu [3]

1   Department of Pathology & Laboratory Medicine, Richard L. Roudebush Veterans Affairs Medical Center, Indianapolis, IN 46202, USA
2   Department of Pathology & Laboratory Medicine, Indiana University School of Medicine, Indianapolis, IN 46202, USA; ederryel@iu.edu
3   Department of Medical & Molecular Genetics, Indiana University School of Medicine, Indianapolis, IN 46202, USA; xxuei@iu.edu (X.X.); ffang@indiana.edu (F.F.); hongao@iu.edu (H.G.); yunliu@iu.edu (Y.L.)
*   Correspondence: raymond.konger@va.gov; Tel.: +1-317-988-2859

Abstract: Given the importance of peroxisome proliferator-activated receptor (PPAR)-gamma in epidermal inflammation and carcinogenesis, we analyzed the transcriptomic changes observed in epidermal PPARγ-deficient mice (*Pparg*-/-^{epi}). A gene set enrichment analysis revealed a close association with epithelial malignancy, inflammatory cell chemotaxis, and cell survival. Single-cell sequencing of *Pparg*-/-^{epi} mice verified changes to the stromal compartment, including increased inflammatory cell infiltrates, particularly neutrophils, and an increase in fibroblasts expressing myofibroblast marker genes. A comparison of transcriptomic data from *Pparg*-/-^{epi} and publicly available human and/or mouse actinic keratoses (AKs) and cutaneous squamous cell carcinomas (SCCs) revealed a strong correlation between the datasets. Importantly, PPAR signaling was the top common inhibited canonical pathway in AKs and SCCs. Both AKs and SCCs also had significantly reduced *PPARG* expression and PPARγ activity z-scores. Smaller reductions in *PPARA* expression and PPARα activity and increased *PPARD* expression but reduced PPARδ activation were also observed. Reduced PPAR activity was also associated with reduced PPARα/RXRα activity, while LPS/IL1-mediated inhibition of RXR activity was significantly activated in the tumor datasets. Notably, these changes were not observed in normal sun-exposed skin relative to non-exposed skin. Finally, *Ppara* and *Pparg* were heavily expressed in sebocytes, while *Ppard* was highly expressed in myofibroblasts, suggesting that PPARδ has a role in myofibroblast differentiation. In conclusion, these data provide strong evidence that PPARγ and possibly PPARα represent key tumor suppressors by acting as master inhibitors of the inflammatory changes found in AKs and SCCs.

Keywords: peroxisome proliferator-activated receptor; inflammation; tumor suppression; non-melanoma skin cancer; actinic keratoses; cutaneous squamous cell carcinoma; transcriptomics; gene set enrichment analysis

1. Introduction

PPARs are members of a large family of related ligand-activated nuclear receptors that bind to a common consensus recognition sequence in the promoters of target genes, the peroxisome proliferators response element (PPRE). The ligand-induced activation of PPARs bound to the PPRE subsequently induces target gene transcription (for review, see [1]). Three different PPAR proteins have been identified (PPARα, PPARδ, and PPARγ), all of which require heterodimerization with the retinoid X receptor α (RXRα) for PPRE binding and transcriptional activity [1]. Endogenous PPAR ligands include unsaturated and saturated fatty acids and fatty acid metabolites [2,3]. While the three different PPAR receptors

exhibit differences in tissue distribution, all three PPARs are known to be expressed in human and mouse skin [4]. In addition, all three PPAR subtypes play key roles as homeostatic regulators of lipid metabolism, energy balance, and cellular differentiation [2,3].

In addition to its role as a direct transcriptional regulator of genes involved in energy balance and lipid metabolism, PPARγ acts through mechanistically distinct transrepressive signaling pathways to suppress the activities of other transcription factors, such as NF-κB, activator protein 1 (AP-1), and the nuclear factor of activated T cells (NFAT) [5]. Using a whole transcriptomic analysis of differentially expressed genes in *Pparg-/-*[epi] relative to wildtype control mice, we showed that *Pparg-/-*[epi] mice exhibit a marked increase in inflammatory mediators and gene products associated with inflammasome activation, indicating that PPARγ has a key role as an important immune modulator [6]. The mice also developed spontaneous inflammatory skin lesions [6]. PPARγ was seen to have a role as a suppressor of cutaneous inflammation in studies of inflammatory dermatoses. Relative to normal human control skin, PPARγ transcripts in psoriatic and atopic lesions are reduced by 8- and 3.3-fold, respectively [7]. Another study demonstrated that *PPARG* mRNA is significantly decreased in human lichen planopilaris, a form of scarring (cicatricial) alopecia [8].

PPARs have also received interest for their potential role in neoplastic development. The keratinocyte-specific loss of *Pparg* in mice *(Pparg-/-*[epi] mice) results in increased photocarcinogenesis and photoinflammation [9], as well as a severe defect in normal contact hypersensitivity (CHS) responses [10]. Similarly, the epidermal-specific loss of either *Pparg* or its heterodimeric partner RXRα in mice resulted in an approximately 2-fold increase in DMBA/PMA-induced tumors [11]. DMBA treatment in mice with hemizygous germline loss of *Pparg* resulted in a cancer incidence increase of over 3-fold, while metastatic disease increased by 4.6-fold [12]. The increase in cancers included a 1.7-fold increase in cutaneous papilloma multiplicity.

In addition to these loss-of-function models, pharmacologic gain-of-function studies also indicate the potential role of PPARγ agonists in cutaneous malignancy. The treatment of mice with rosiglitazone was shown to suppress chemical carcinogenesis by approximately 70% [13]. Rosiglitazone also blocks the ability of ultraviolet light to suppress both CHS responses and anti-tumor immunity [10]. In addition, rosiglitazone promotes anti-tumor immune reactions in a mouse immunogenic cutaneous SCC tumor model [14]. In yet another study, the anti-neoplastic efficacy of immune therapy consisting of CTLA4 blockade and a cancer vaccine was enhanced by the addition of rosiglitazone treatment [15]. Collectively, these data indicate a potential tumor suppressor role of PPARγ that is mediated by its effects on inflammation and anti-tumor immune responses.

Chronic inflammation and immunosuppression are hallmarks of the tumor microenvironment [16,17]. While malignant tumors orchestrate changes to the stromal microenvironment to promote tumor growth and escape from immune surveillance, it is unclear how this process is regulated. Mice lacking epidermal *Pparg* (*Pparg-/-*[epi] mice) also exhibit immune suppression, chronic inflammation, and increased chemical and photocarcinogenesis. We were therefore interested in determining whether the transcriptomic changes observed in *Pparg-/-*[epi] mice exhibit any overlap with non-melanoma skin cancer (NMSC). We utilized a transcriptomic analysis and single-cell RNA sequencing (scRNAseq) to provide evidence that PPAR signaling is the top inhibited canonical signaling pathway in NMSC and that this loss correlates with significant reductions in PPARγ expression and activity and increased cytokine and chemokine signaling. Smaller but significant reductions in PPARα mRNA expression and activity were also seen, suggesting a potential tumor suppressor role for PPARα as well. In *Pparg-/-*[epi] mice, scRNAseq further indicated that epidermal *Pparg* is a key epidermal regulator that modulates the recruitment of stromal myeloid, lymphoid, and fibroblast populations.

2. Materials and Methods

2.1. Animal Studies

The derivation of mice lacking epidermal *Pparg* in the C57BL/6 background (*Pparg-/-*epi) and wildtype controls (lacking Cre recombinase) was previously described [10]. Mice were housed under specific pathogen-free conditions at the Indiana University School of Medicine.

2.2. Whole Transcriptomic mRNA Sequencing

mRNA sequencing and a subsequent differentially expressed gene analysis were performed on epidermal scrapings of *Pparg-/-*epi mice relative to wildtype controls as previously described [6]. Sequencing was carried out on RNA obtained from the skin of 6 mice per genotype [6]. In this previously published study, we characterized how changes in gene expression correlated with the phenotypic changes that we observed in *Pparg-/-*epi mice. This included spontaneous inflammatory skin lesions, an asebia phenotype, and epidermal permeability defects. This dataset is also publicly available at the Gene Expression Omnibus (GEO), National Center for Biotechnology Information (NCBI) depository (accession number: GSE164024).

2.3. Single Cell Isolation

Two mice (one male and one female) were euthanized for each genotype (wildtype and *Pparg-/-*epi). Dermal and epidermal cells were isolated from areas of telogen phase hair cycling for each mouse. For dermal cell preparation, the tissues were minced and digested in 2.5 mg Liberase TM, 16.7 mg DNase I, penicillin, and streptomycin in RPMI media (all reagents from Sigma-Aldrich, St. Louis, MO, USA) for 90 min at 37 °C. The digest was filtered through a 40 μm filter. After adding 5 mL of ice-cold dialyzed FBS, the samples were centrifuged at $300\times g$ for 10 min. RBC lysis (RBC Lysis Buffer, Cat #00-4333-57, ThermoFisher Scientific, Waltham, MA, USA) followed by dead cell removal (dead cell removal kit #130-090-101, Miltenyi Biotec, Auburn, CA, USA) with centrifugation were performed after each step. The cell prep was washed twice with cell suspension buffer [PBS (calcium, magnesium, DNase, and RNase free) (Catolog # 40120706, bioWORLD, Dublin, OH, USA) containing 1% BSA] followed by centrifugation. RNA sequencing was then performed on a final cell prep resuspended in cell suspension buffer containing 0.5 U/μL SUPERaseIn™ RNase Inhibitor (Catalog #AM2694, ThermoFisher Scientific, Waltham, MA, USA) and 0.5 U/μL Protector RNase Inhibitor (Catalog #3335399001, Sigma-Aldrich, St. Louis, MO, USA).

For epidermal cell preps, the dermal fat and dermis were removed using a scalpel, and the epidermal sheet was suspended in dispase II solution Sigma-Aldrich, St. Louis, MO, USA) for 2 hrs at 37 °C. After suctioning the dispase and scraping the epidermis from the dermis, the tissue was rinsed with PBS, centrifuged, and incubated in 5 mL Accutase solution (Cat# CnT-Accutase-100, CELLnTEC Advanced Cell Systems, Bern, Switzerland) for 20 min at room temp. After filtering through a 70 μm filter, 5 mL of dialyzed FBS was added, and the cells were pelleted by centrifugation. Dead cell removal and further processing were then performed as described for the dermal cell prep. The epidermal cells and dermal cells were then recombined at a 1:10 ratio (dermal vs. epidermal), and the male and female cells were pooled together.

2.4. Single-Cell Sequencing and Library Prep Protocol

After evaluating for cell number, cell viability, and cell size, the appropriate number of cells were loaded on a multiple-channel micro-fluidics chip of the Chromium Single-Cell Instrument (10x Genomics, Pleasanton, CA, USA) with a targeted cell recovery of 10,000. Single-cell gel beads in emulsion containing barcoded oligonucleotides and reverse transcriptase reagents were generated with the v3.1 Next GEM Single Cell 3′ reagent kit (10X Genomics, Pleasanton, CA, USA). Following cell capture and cell lysis, cDNA was synthesized and amplified. An Illumina sequencing library was then prepared with the amplified cDNA with the Chromium™ Next GEM Single-Cell 3′ GEM, Library & Gel

Bead Kit v3.1 (10X Genomics, Pleasanton, CA, USA). The resulting library was sequenced, including cell barcode and UMI sequences, and 100 bp RNA reads were generated with Illumina NovaSeq 6000 (Illumina, San Diego, CA, USA) at the Center for Medical Genomics of the Indiana University School of Medicine.

2.5. Analysis of scRNAseq Data

CellRanger 6.1.1 (http://support.10xgenomics.com/ 10X Genomics, Pleasanton, CA, USA. Accessed on 7 January 2022) was utilized to process the raw sequence data generated. Briefly, cellranger mkfastq was implemented to demultiplex raw base sequence calls generated from the Illumina sequencer into sample-specific FASTQ files. The FASTQ files were then aligned to the mouse reference genome mm10 with RNAseq aligner STAR. The aligned reads were traced back to individual cells, and the gene expression level of individual genes were quantified based on the number of UMIs (unique molecular indices) detected in each cell. The filtered feature-cell barcode matrices generated using CellRanger were used for further analysis.

2.6. SoupX Analysis

The R package SoupX version 1.5.2 [18] was used to remove cell-free contaminating RNA from the data.

2.7. Seurat Analysis

The R package Seurat version 4.0 [19–22] was used for the following analyses: cell type/state discovery with graph-based clustering, cell cluster marker gene identification, and various visualization. A QC metrics of the library size, number of features/genes, and mitochondrial reads (based on median absolute deviation (MAD); MAD of 3 used here) was calculated with Scater [23]. This, together with the QC analysis in Seurat, were used to determine the parameters used for excluding low-quality cells.

2.8. Performing QC and Selecting Cells for Further Analysis

Low-quality cells were excluded with the following criteria: cells with unique feature/gene counts over 7000 or less than 300 or >10% reads mapped to mitochondrial genome. A summary of the final scRNAseq data output is shown in Figure S1 (WT mouse cells) and Figure S2 (*Pparg*-/-epi mouse cells).

2.9. Unsupervised Cell Cluster Segregation and Cluster Identification

Unsupervised clustering was performed using Loupe Browser software (v6.5.0; 10x Genomics, Pleasanton, CA, USA) by uniform manifold approximation and projection (UMAP). Using Loupe Browser, DEGs for each individual cell cluster were obtained. The cell type within each cluster was identified by uploading the top differentially expressed genes for each cluster into the Enrichr online analysis application [24–26] and then cross-referencing with the PanglaoDB database [27].

2.10. GTEX Data Analysis

Tissue-specific (sun-exposed lower leg skin and sun-protected suprapubic skin) TPM for *PPARA*, *PPARD*, and *PPARG* were downloaded from the GTEX portal [www.gtexportal.org]. After uploading the TPM data, differential expression for the PPARs was calculated using edgeR (DEApp website: yanli.shinyapps.io/DEApp/. Accessed 6 December 2023) [28].

2.11. Gene Set Enrichment Analysis

Ingenuity Pathway Analysis (IPA) was performed to identify predicted diseases and biofunctions, canonical pathways, and upstream regulators that are enriched in datasets relative to what would be expected by chance (QIAGEN Inc., Germantown, MD, USA. https://digitalinsights.qiagen.com/IPA, Accessed 6 December 2023) [29].

3. Results

3.1. The Transcriptomic Changes in Pparg-/-^{epi} Mice Show a Strong Correlation to Inflammatory Cell Recruitment and Mobilization

To better understand how the loss of epidermal *Pparg* reflects disease processes, we reanalyzed our transcriptomic dataset from *Pparg*-/-^{epi} mouse skin and wildtype mouse skin (GSE164024, [6]). After obtaining the list of differentially expressed genes (DEGs) that we observed in *Pparg*-/-^{epi} mouse skin relative to wildtype mouse skin, we uploaded this dataset into Ingenuity Pathway Analysis (IPA, Qiagen, Germantown, MD, USA) and then performed a gene set enrichment (GSE) analysis for diseases and biofunctions (the complete annotated list is in Table S1).

A potential clue of how PPARγ could influence cancer is seen in Table 1, in which the top 20 matching disease and biofunction terms are shown after sorting by the highest positive activation z-scores. All 20 had activation z-scores of 3.942 to 5.052, well above the 2.0 cutoff that is used to predict activation. Of these, 15 of the biofunctions were associated with inflammatory cell homing, chemotaxis, or the inflammatory response. The remaining biofunctions were related to cell viability, tumor or cell invasion, and the growth of lesions or tumors. Given the important role of inflammation in cancer, these data suggest that the primary interaction of PPARγ in tumor development may center on its anti-inflammatory activity. Overall, this approach found a strong linkage to inflammatory biofunctions, as shown in Table 1.

Table 1. The top 20 disease or biofunction terms that match with the DEG dataset from *Pparg*-/-^{epi} mouse skin relative to WT skin (sorted by z-score).

Disease or Biofunction Annotation	*p*-Value	Activation z-Score
Chemotaxis of leukocytes	1.61×10^{-12}	5.052
Homing of leukocytes	8.69×10^{-14}	4.724
Cell movement of tumor cell lines	3.36×10^{-11}	4.686
Chemotaxis	2.68×10^{-18}	4.644
Migration of cells	1.13×10^{-30}	4.623
Homing of blood cells	4.72×10^{-14}	4.574
Cell survival	2.9×10^{-15}	4.568
Leukocyte migration	2.98×10^{-29}	4.468
Cell movement	2.97×10^{-37}	4.464
Cell movement of blood cells	1.82×10^{-29}	4.36
Invasion of cells	9.29×10^{-15}	4.359
Homing of cells	3.91×10^{-21}	4.249
Inflammatory response	9.14×10^{-20}	4.174
Cell movement of myeloid cells	2.13×10^{-18}	4.171
Recruitment of myeloid cells	1.19×10^{-13}	4.121
Cell viability	1.77×10^{-14}	4.086
Recruitment of blood cells	3.44×10^{-19}	4.07
Cell movement of phagocytes	5.77×10^{-19}	4.029
Growth of lesion	5.78×10^{-30}	3.992
Growth of tumor	1.15×10^{-29}	3.942

3.2. Single-Cell Sequencing of Pparg-/-^{epi} Mice Reveals Increase in Immune Cells, Particularly Neutrophils

To determine how the loss of epidermal *Pparg* alters the stromal immune environment, we next performed single-cell sequencing of skin from both the WT and *Pparg*-/-^{epi} mice. We found that 1560 genes were differentially expressed in the *Pparg*-/-^{epi} cells relative to the WT cells (Figure 1A; a full list of DEGs can be found in Table S2). Of these, 94.9% of the DEGs were shared with the DEGs found in our previous whole transcriptomic RNAseq dataset [6]. After an unsupervised cluster analysis, 26 different cell clusters were identified (Figure 1B). Table S3 shows the Enrichr analysis for the cell types found in each cell cluster. After focusing on non-cytokeratin-expressing cells, we found that 44.11% of

non-keratinocytes represented *Ptprc* (CD45)-expressing immune cells in *Pparg-/-*epi mouse skin (Figure 1C and Table S3). In contrast, 20.42% of non-keratinocytes were *Ptprc*+ in the WT mouse skin (Figure 1C and Table S3). This increase in immune cells in *Pparg-/-*epi mouse skin relative to other stromal cell types was reflected as an increase in both myeloid and lymphoid cell populations (Figure 1C).
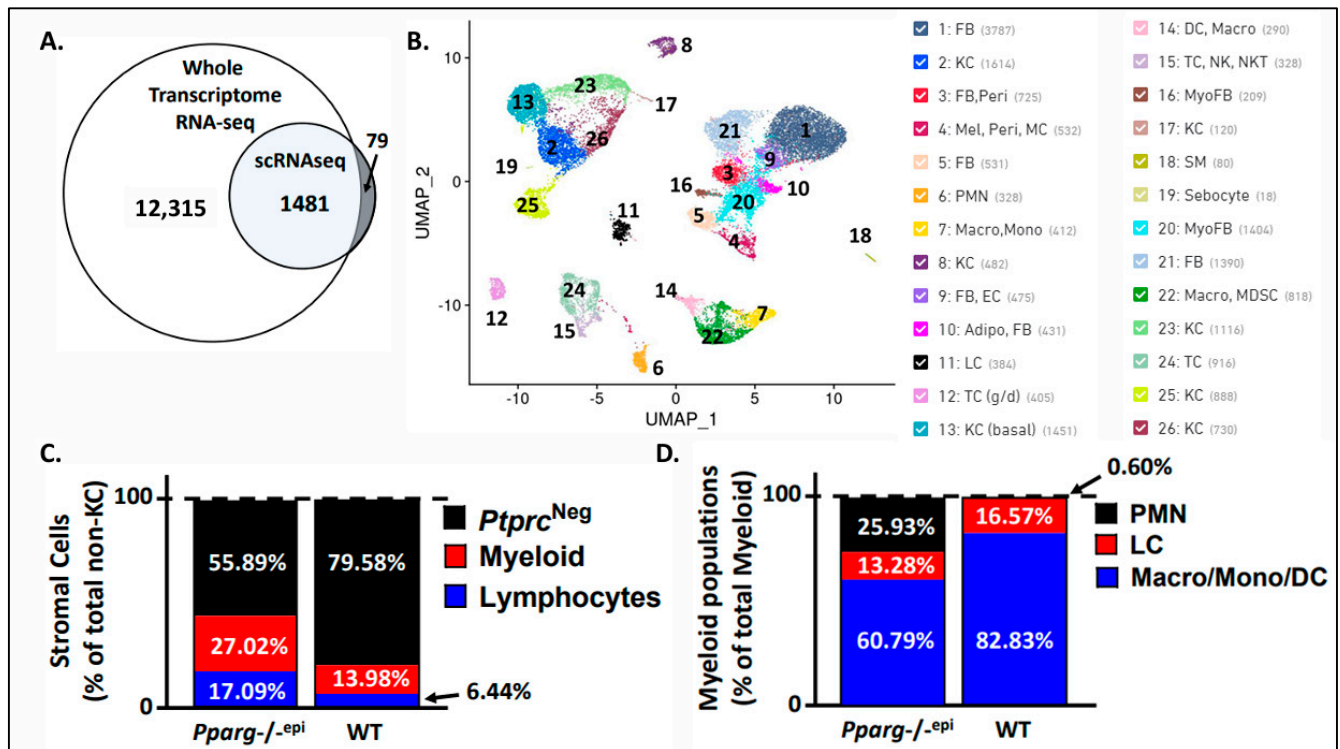

Figure 1. Single-cell sequencing reveals changes in the dermal cell infiltrate in *Pparg-/-*epi mice. (**A**) A Venn diagram showing the overlap between differentially expressed genes (DEGs) from whole transcriptomic RNA sequencing (RNA-seq) and from the single-cell RNA sequencing (scRNAseq) of *Pparg-/-*epi mouse skin. While scRNAseq suffers from reduced sensitivity, thus resulting in a much smaller number of DEGs, 94.94% of the DEGs identified by scRNAseq were also identified as DEGs by whole transcriptomic RNA-seq. (**B**) An unsupervised cell cluster analysis using uniform manifold approximation and projection (UMAP) depicts 26 cell clusters that are present in both WT and *Pparg-/-*epi mouse skin. FB: fibroblasts; KC: keratinocytes; Peri: pericytes; Mel: melanocytes; MC: mast cells; PMN: polymorphonuclear cells; Macro: macrocytes; Mono: monocytes; EC: endothelial cells; Adipo: adipocytes; LC: Langerhans cells; TC (g/d): γδ T-lymphocytes; DC: dendritic cells; NK: natural killer cells; NKT: natural killer T-lymphocytes; MyoFB: myofibroblasts; SM: smooth muscle; MDSC: myeloid-derived suppressor cells. (**C**) Cytokeratin-negative stromal cells from either WT or *Pparg-/-*epi skin were subdivided into CD45 (*Ptprc*)-positive and *Ptprc*-negative (*Ptprc*Neg) cell populations. *Ptprc*-positive immune cells were subdivided into *Cd3*-positive lymphocyte and *Cd3*-negative myeloid populations. The different populations are depicted as a percentage of total stromal cells. (**D**) The myeloid populations were further subdivided into a granulocytic (PMN) population, Langerhans cell population, and a pooled population of non-granulocytic macrophages, monocytes, and dendritic cells (Macro/Mono/DC). Each population is shown as a percentage of total myeloid cells.

After a further analysis of only the myeloid cell populations, we found that neutrophils represented only 0.6% of the total myeloid cell population observed in the WT mice (Figure 1D and Table S3). This low neutrophil count is not particularly surprising as neutrophils are infrequent in normal mouse skin [30]. In contrast, neutrophils represented

25.93% of the total myeloid cell population in *Pparg*-/-^epi^ mice, which is a 43-fold increase relative to the WT mice (Figure 1D).

3.3. Fibroblasts Expressing Myofibroblast Markers Are Increased in Pparg-/-^epi^ Mouse Skin

In addition to differences in immune cell clusters, we also found differences in the stromal fibroblasts from *Pparg*-/-^epi^ mouse skin. In Figure 2A, we show the expression of the collagen type I alpha 2 gene (*Col1a2*) in non-immune stromal cell clusters. Clusters 16 and 20, along with clusters 1, 3, 5, 9, 10, and 21, expressed high levels of *Col1a2*, consistent with the Enrichr identification of these clusters as fibroblasts. Also as expected, *Col1a2* gene expression was absent in clusters representing primarily melanocytes and mast cells (cluster 4) and smooth muscle cells (cluster 18).
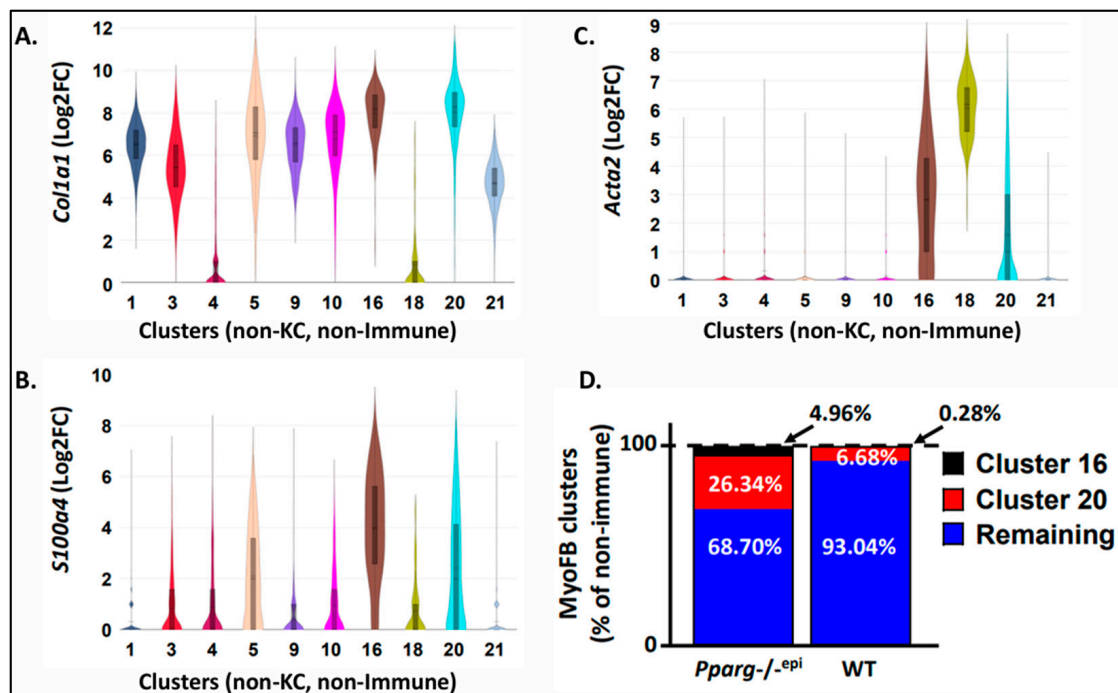

Figure 2. Fibroblast clusters expressing myofibroblast gene markers are increased in *Pparg*-/-^epi^ mouse skin. (**A–C**) Violin plots showing the log 2 fold change (Log2FC) of the following genes that were expressed in both cytokeratin-negative and CD45 (*Ptprc*)-negative stromal cell clusters: (**A**) alpha-1 type I collagen (*Col1a1*), (**B**) S100 calcium-binding protein A4 (*S100a4*), and (**C**) smooth muscle actin 2 (*Acta2*). (**D**) The percentages of cluster 16 and 20 fibroblasts that are enriched in the expression of myofibroblast (MyoFB) markers as a percentage of total non-immune stromal cells are shown for both WT and *Pparg*-/-^epi^ mouse skin.

The Enrichr analysis indicated that clusters 16 and 20 have differential gene expression overlap with pancreatic stellate cells (PSCs) (Table S3). As activated PSCs are highly fibrogenic myofibroblasts (myoFBs) [31], we verified that these fibroblast clusters express myofibroblast-specific genes. Figure 2B,C show the expression of S100 calcium binding protein A4 (*S100a4*) [also known as fibroblast specific protein 1] and alpha smooth muscle actin (*Acta2*), respectively. Both *S100a4* and *Acta2* are expressed in mouse dermal myofibroblasts, although *Acta2* is the more specific marker [32]. Only fibroblast clusters 16 and 20 expressed both markers, with the expression being particularly high in cluster 16. As an internal positive control, *Acta2* was highly expressed in the smooth muscle cell cluster (cluster 18).

In Figure 2D, we show that cluster 16 myofibroblasts were infrequent in the WT dermis (0.28% of non-immune stromal cells). In contrast, cluster 16 myofibroblasts were enriched in *Pparg-/-*epi mice, representing nearly 5% of non-immune stromal cells (relative fold change of 17.7-fold over WT mice). Similarly, cluster 20 myofibroblasts were enriched by nearly 4-fold in *Pparg-/-*epi mouse skin (26.34% vs. 6.68% of non-immune stromal cells in *Pparg-/-*epi and WT skin, respectively).

3.4. The GSE Analysis Reveals Strong Similarity between the Pparg-/-epi Transcriptomic Data and That of Human Actinic Disease and Mouse and Human SCCs

To verify that the chronic inflammatory microenvironment observed in *Pparg-/-*epi mice is relevant to non-melanoma skin cancer, we uploaded DEG datasets for both our whole transcriptomic RNAseq [6] and the single-cell RNAseq (Table S1) for the IPA. We also uploaded DEGs for publicly available transcriptomic datasets of human actinic keratoses (AKs), human SCCs, and mouse SCCs (relative to normal skin). (Details of the publicly available datasets can be found in Table S4.) To determine how closely the *Pparg-/-*epi datasets correlate with the different tumor datasets, we performed a comparison analysis of diseases and biofunctions.

Figure 3A,B show heatmaps that demonstrate the different disease and biofunction processes that are significantly associated with the datasets, and they are sorted by z-score. Figure 3A is limited to a comparison between *Pparg-/-*epi mouse skin data and human AK or SCC datasets, while Figure 3B compares *Pparg-/-*epi data to that of mouse SCC. Both the whole transcriptomic and single-cell RNA sequencing datasets for *Pparg-/-*epi mice were largely in agreement, with the observed differences generally being associated with the non-informative z-scores (z-score near 0) in the scRNAseq dataset due to the much smaller DEG profile for this less sensitive technique. For the tumor datasets, the activating scores varied but were largely in agreement across datasets. As with the two different *Pparg-/-*epi datasets, the greatest differences across the different tumor datasets were largely due to non-informative terms. In addition, no consensus was seen for "Organismal death", which was predicted to be activated, inhibited, or not effected depending on the dataset. Surprisingly, the correlation between *Pparg-/-*epi mouse skin and human AKs and SCCs (Figure 3A) was stronger than that between *Pparg-/-*epi mice and mouse cutaneous SCCs (Figure 3B). When the *Pparg-/-*epi mouse dataset was compared to that of mouse SCCs, there were more non-informative functions observed in the *Pparg-/-*epi dataset compared to the mouse tumor datasets.

Given that *Pparg-/-*epi mice are highly susceptible to cutaneous carcinogenesis, it is particularly interesting that there was close agreement between the *Pparg-/-*epi transcriptomic datasets with the tumor datasets. In both Figure 3A,B, the activating z-scores for functional annotations associated with cell movement, chemotaxis, and cell invasion were strongly associated with both the *Pparg-/-*epi and tumor datasets. Other functions that were activated in most datasets included various functions associated with cell viability, tumor growth, tumor invasion, and metastasis.

BCCs represent the most common NMSC observed in humans. We therefore also ran a correlation GSE analysis of our *Pparg-/-*epi datasets with six human BCC transcriptomic datasets (Figure S3). As BCCs are not found in mice lacking disruptions in patched signaling, it is not surprising that there was a limited correlation between the diseases and biofunction annotations that were common to both the *Pparg-/-*epi dataset and the BCC datasets. However, in contrast to the AK and SCC datasets, there was considerable discordance for the disease and biofunctions linked to different BCC datasets. This could indicate a greater degree of tumor heterogeneity in BCCs. Poor predictive modeling could also be due to a reduced number of gene expression changes or more modest effect size changes in the DEGs associated with indolent BCCs.
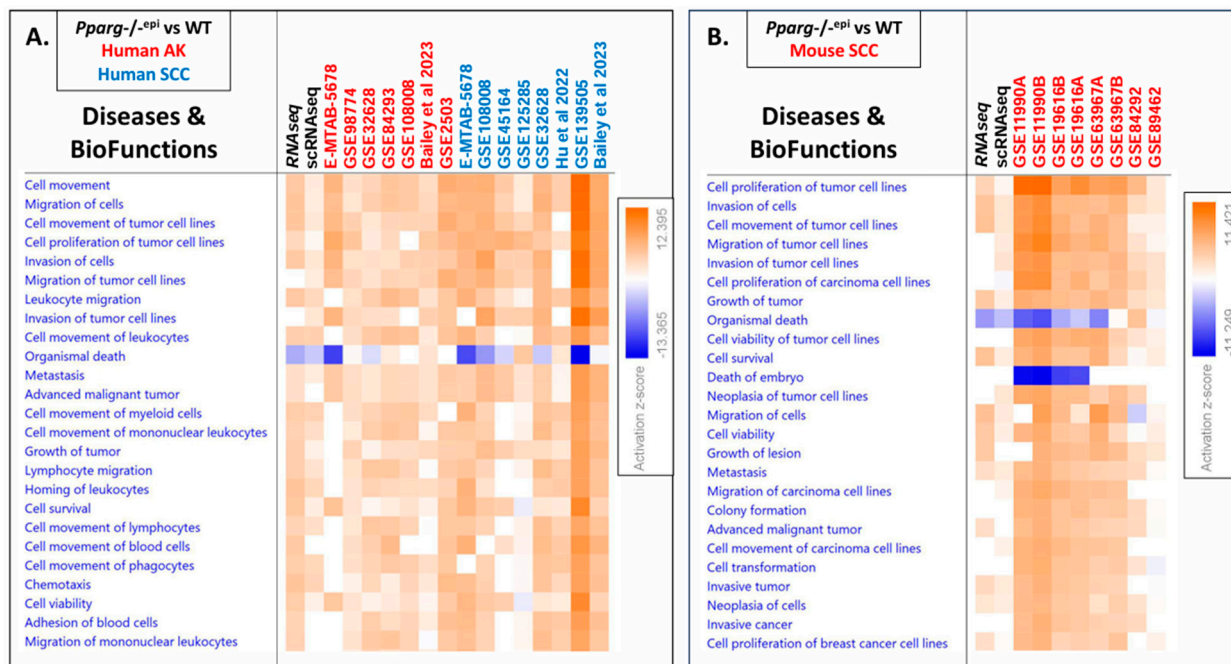
Figure 3. A heat map showing the top common diseases and biofunctions that are mapped to the differentially expressed genes found in *Pparg-/-*epi mice, human actinic keratoses (AKs), human squamous cell carcinomas (SCCs), and mouse SCCs. Differentially expressed genes from the whole transcriptomic RNA sequencing (RNAseq) and single-cell RNA sequencing (scRNAseq) were obtained for *Pparg-/-*epi relative to the WT mice. (**A**) The DEGs from these two datasets, as well as the DEGs obtained from publicly available human AK and SCC tumor databases (Table S4), were uploaded for Qiagen's Ingenuity Pathway Analysis. A comparison analysis was performed, and the top 25 diseases and biofunctions that were mapped to the various databases are shown and ranked by activation z-score. (**B**) A comparison heat map showing the top 25 diseases and biofunctions that are common to both the DEGs from *Pparg-/-*epi mouse skin and mouse SCC transcriptomic datasets.

3.5. The Canonical Pathway Analysis Shows that the Loss of PPAR Signaling Is a Top Inhibited Canonical Pathway in Human AKs, Human SCCs, and Mouse SCCs

To determine whether similarities in diseases and biofunctions are associated with common signaling pathways, we utilized an IPA to compare the canonical pathways that are predicted to be activated or inhibited based on the DEGs found in *Pparg-/-*epi mouse skin and those from human AKs or SCCs (Figure 4A), as well as a comparison with both human and mouse SCCs (Figure 4B). As with diseases and biofunctions, there was a relatively high level of consistency in the z-scores between the pathways mapped to *Pparg-/-*epi mouse skin and human tumors (Figure 4A). Canonical pathways with largely positive z-scores were heavily associated with cytokine and chemokine signaling, innate and adaptive immune responses, pyroptosis, the tumor microenvironment, and fibrosis. These changes are not surprising given the known role of inflammation in tumor–stroma interactions.

The strong correlation between the predicted activation of these pathways in both malignancy and *Pparg-/-*epi mouse skin further supports the potential role of PPARγ as a tumor-suppressing signal through its anti-inflammatory activity. It is therefore of interest that "PPAR Signaling" was the top common canonical pathway, which shows largely negative z-scores in Figure 4A. Interestingly, the canonical pathway "LPS/IL-1 Mediated inhibition of RXR Function" was predicted to be activated in most of the AK and SCC datasets. This is of interest as the inhibition of RXRα activity could indirectly impact PPAR signaling as all PPARs require heterodimerization with RXRα for their transcriptional activity. In addition, as noted above, LPS and IL1β signaling also directly inhibit *PPARG/Pparg* transcript expression and target gene expression [33]. Thus, the activation of this pathway can suppress PPARγ signaling both directly and indirectly.
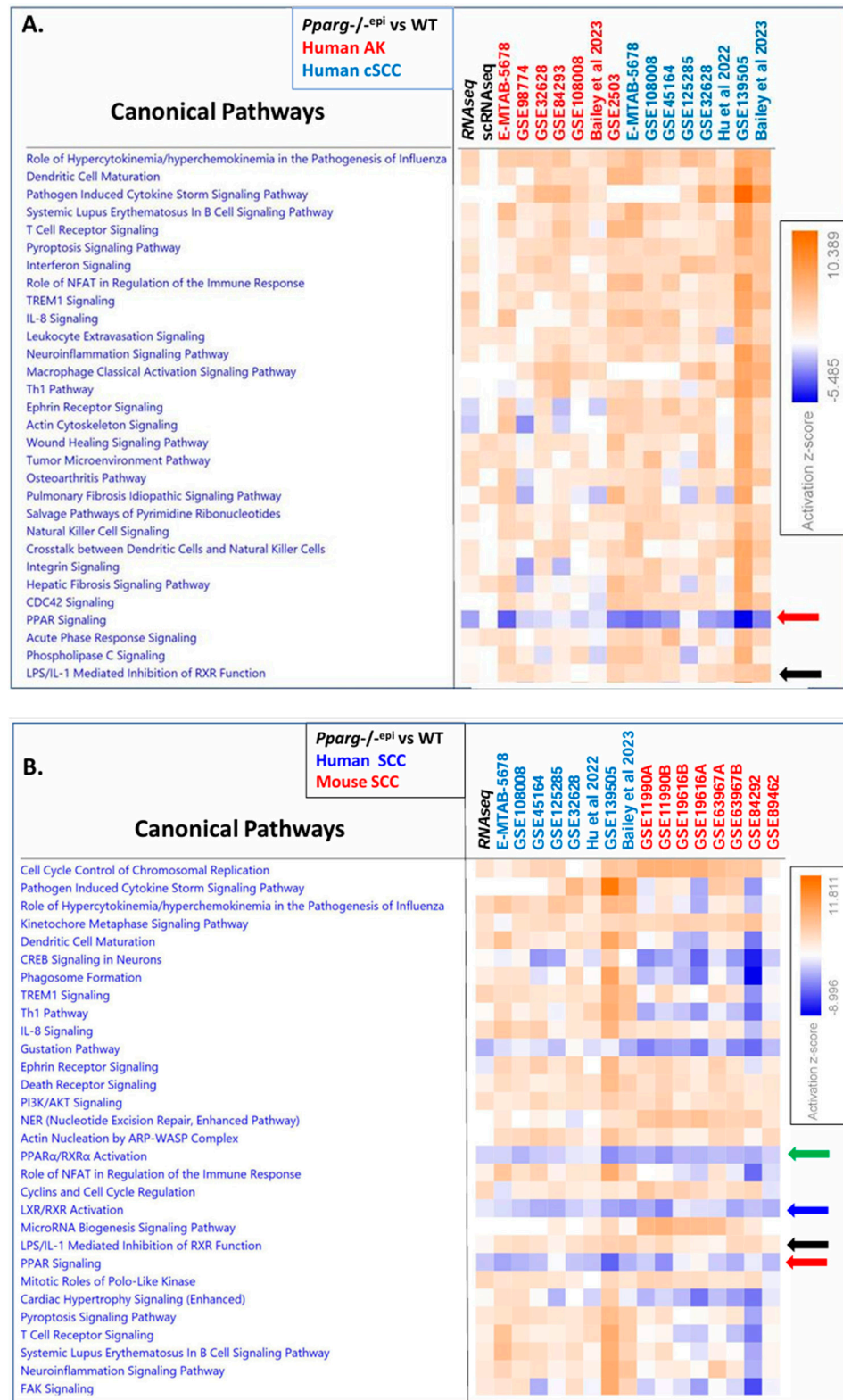
Figure 4. Heat maps showing top common canonical pathways that are mapped to the differentially expressed genes found in *Pparg-/-*^epi mice, human actinic keratoses (AKs), human squamous cell carcinomas (SCCs), and mouse SCCs. (**A**,**B**) The data analyzed in Figure 3 were further analyzed for common canonical pathways using an IPA. The canonical pathways in (**A**,**B**) are marked as follows: "PPAR Signaling" is marked by the red arrow. "LPS/IL-1 Mediated inhibition of RXR Function" is marked by the black arrow. The green arrow marks "PPARα/RXRα Activation", and the blue arrow

marks "LXR/RXR Activation". (**A**) The top 30 canonical pathways that were mapped to the *Pparg*-/-^epi^ mouse and human AK and SCC databases are shown and ranked by activation z-score. (**B**) The top 30 canonical pathways that are common to the *Pparg*-/-^epi^ mouse skin, human SCC, and mouse SCC, transcriptomic datasets are shown (ranked by z-score).

In Figure 4B, we show a similar heat map that illustrates common canonical pathways that are activated or inhibited in *Pparg*-/-^epi^ mouse skin and either human or mouse SCCs. As with Figure 4A, the canonical pathway "PPAR Signaling" showed largely negative z-scores in all SCC datasets. In addition, several additional canonical pathways linked to PPAR signaling were also inhibited. The "PPARα/RXRα activation" and "LXR/RXRα activation" canonical pathways were also predicted to be inhibited in *Pparg*-/-^epi^ mouse skin and the tumor datasets. The predicted suppression of signaling by these two heterodimeric partners of RXRα is consistent with the predicted activation of the "LPS/IL-mediated inhibition of RXR signaling" that we observed in the human AK and SCC datasets (black arrows in Figure 4A,B).

As with the diseases and biofunctions in Figure 3, there was more disagreement in the canonical pathways between the *Pparg*-/-^epi^ mouse skin RNAseq data relative to the mouse SCCs than there was between the *Pparg*-/-^epi^ mice and human SCCs (compare Figure 4A,B). These differences included positive z-scores for canonical pathways such as "Phagosome Formation", "Role of NFAT in Regulation of the Immune Response", "T cell receptor signaling", and "FAK Signaling" for *Pparg*-/-^epi^ mice and human SCCs, but there was a trend of negative z-scores for these canonical pathways in mouse SCCs.

Finally, we also examined canonical signaling pathways in human BCCs (Figure S4). As with the diseases and biofunctions analysis, canonical signaling pathways that were annotated to the *Pparg*-/-^epi^ mouse or BCC datasets showed a poor consensus. This suggests that the gene expression changes that occur with the loss of epidermal *Pparg* may not be particularly relevant to the top canonical signaling pathways that are observed in BCCs.

3.6. A Shift to Reduced PPAR and RXR Activity and Reduced PPARA/Ppara and PPARG/Pparg Expression but Increased PPARD/Ppard Expression Occurs during the Progression from Sun-Exposed Skin to NMSC

Given that PPAR and RXR signaling represent the top inhibited canonical signaling pathways in Figure 4A,B, we further examined how PPAR signaling, PPARα/RXRα activation, and the LPS/IL1-mediated inhibition of the RXR function were altered during tumor progression.

In Figure 5A, we plot the mean z-scores for the canonical pathway "PPAR Signaling" for the human and mouse tumor dataset as well as human sun-exposed skin (hSES). For hSES relative to non-sun-exposed skin (NES), "PPAR Signaling" had significantly positive mean z-scores near the z-score activation cutoff of 2.0. In contrast, the mean z-scores were significantly reduced for human AKs, human SCCs, and mouse SCCs. In all three cases, the means were near the inhibitory z-score threshold of −2.0. The shift from a positive "PPAR Signaling" z-score in SES to a negative z-score in human SCC was also statistically significant.

In Figure 5B, the mean z-scores for the canonical pathway "PPARα/RXRα Activation" are similarly shown. In the case of SES vs. NES, the datasets were non-informative, indicating no impact on the canonical pathway "PPARα/RXRα activation". However, negative mean z-scores were observed for human AK, human SCC, and mouse SCC. Again, the mean z-score for human BCCs was not significantly different from zero.

Figure 5C shows the z-score distribution for the different tumor types when the canonical pathway "LPS/IL1-mediated inhibition of RXR function" was plotted. Again, the SES vs. NES datasets were non-informative. For human AKs, human SCCs, and mouse SCCs, the mean z-scores were near or exceeded the activation cutoff of 2.0. In contrast to Figure 5A,B, human BCCs showed a significantly positive mean z-score, although this mean score was well below the activation cutoff.
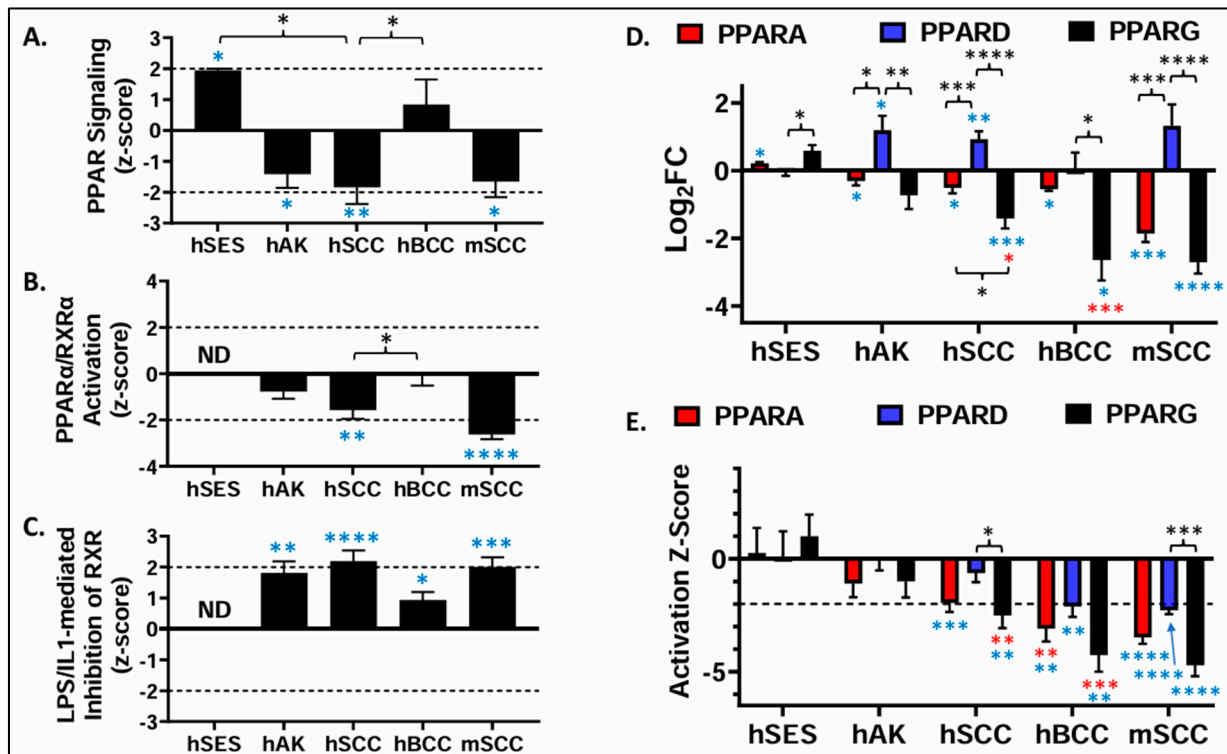
Figure 5. The transcriptomic analysis indicates that PPAR signaling is inhibited, while PPARγ (and PPARα) expression and activity are suppressed in human AKs, human SCCs, and mouse SCCs. (**A–C**) Following GSEA, activation z-scores were obtained for each of the different datasets for the following canonical pathways: (**A**) PPAR signaling, (**B**) PPARα/RXRα activation, and (**C**) LPS/IL1-mediated inhibition of RXR. The plots depict the mean and SEM of the activation z-scores for the different canonical pathways. The hashmark lines represent the cutoff for the predicted activation (2.0 activation z-score) or predicted inhibition (–2.0) of the respective canonical pathway. For the hSES dataset, no predictive z-score was provided for these canonical pathways (ND = no data). (**D**) For each dataset, the mRNA expression for each of the three different PPAR isoforms was obtained as the Log_2 fold change (Log2FC). The data shown are the mean and SEM of the Log_2FC. (**E**) After uploading the DEG data from each tumor or hSES dataset for the IPA, activation z-scores were obtained for PPARα, PPARδ and PPARγ. The data shown are the mean and SEM of the activation z-score for each PPAR isoform. The hashmark line represents the cutoff for the predicted inhibition (−2.0) of the respective PPAR isoform. Blue asterisks = significantly different from zero. One sample T-test. Red asterisks = significantly different from hSES expression (1-way ANOVA). Black asterisks = significantly different from each other (1-way ANOVA). *, $p < 0.05$; **, $p < 0.01$; ***, $p < 0.001$; ****, $p < 0.0001$.

As PPAR isoforms have significant overlap in target genes, the decrease in the canonical pathway PPAR signaling that is seen in Figure 5A could reflect changes in the activity of one or more of the PPARα, PPARδ, or PPARγ isoforms. Moreover, the decrease in PPARα/RXRα the canonical pathway's activation could indicate a reduction in PPARα activation. Alternatively, the increased activation of the canonical pathway "LPS/IL1-mediated inhibition of RXR function" indicates that RXRα activity is likely reduced, a result that would impact the activity of all three PPAR isoforms. We therefore examined PPAR isotype transcript expression in human sun-exposed skin (SES), AKs, human SCCs, and mouse cutaneous SCCs (Figure 5D).

In Figure 5D, the mean *PPARG* expression was increased in SES relative to NES by approximately 1.5-fold. In the premalignant AK and malignant BCC and human SCC datasets, this was reversed: the mean *PPARG* expression was reduced by 39.6% in AKs, 62.3% in SCCs, and 84.0% in BCCs. This change from non-malignant SES was statistically

significant for both the SCC and BCC datasets. In mouse SCCs, *Pparg* expression was also decreased by 84.7% relative to normal skin. The data for *PPARA/Ppara* in Figure 5D were similar in pattern to that observed for *PPARG/Pparg*, although to a lesser degree. However, the reduction in *PPARA* expression for the tumor datasets was not significantly different from that obtained from the SES datasets. In contrast to *PPARA* and *PPARG*, *PPARD* expression was not altered in SES or BCCs, but *PPARD/Ppard* was significantly increased in AKs and both human and mouse SCCs.

A limitation of the analysis in Figure 5D is the relatively small number of studies that reported *PPAR* expression in SES vs. NES. No PPAR expression data were reported in the studies by Kita et al. [34] and Zou et al. [35] (Table S4). However, both studies limited their reported DEGs to those that met both a statistical threshold and a fold change threshold. The absence of all three PPARs in their listed DEGs indicates that PPARs were only modestly or non-significantly altered in SES vs. NES. This idea was further supported by obtaining the GTEX dataset for SES (lower leg) and NES (suprapubic) and performing a differential expression analysis for the PPARs (Table S4). As expected, the changes in *PPAR* expression were modest and none were significant. Thus, a significant alteration in *PPAR* expression is not likely a feature of chronically sun-exposed skin. Thus, a shift to reduced *PPARA* and *PPARG* expression is a feature of premalignant AKs as well as the two most common NMSCs (BCC and SCC). For *PPARD*, this shift is reversed for AKs and SCCs, with a significant increase in expression relative to normal skin.

Interestingly, when we examined *Ppara* and *Ppard* expression in our *Pparg-/-*^{epi} whole transcriptomic dataset, we found that the loss of epidermal *Pparg* resulted in a 60% decrease in *Ppara* expression (FC = -2.482 (FDR = 1.89×10^{-12})) and a 1.5-fold increase in *Ppard* expression (FDR = 2.66×10^{-4}) [6]. It is important to note that in *Pparg-/-*^{epi} mice, the observed changes to *Ppara* expression in the skin are triggered by the loss of *Pparg* only within keratinocytes.

In the tumor datasets, it is unclear whether the observed changes in *PPAR* expression are occurring in the tumor epithelium or stromal cells. To address this question, *PPAR* isotype expression was obtained from a published dataset created by Mitsui et al. [36]. This study obtained transcriptomic data from AKs and SCC but utilized laser capture microdissection to limit the analysis to the epithelial tissue (Table S4). In this case, the pattern of *PPAR* expression was similar to the observed changes in Figure 5D. *PPARA* expression was reduced by 66.6% and 65.7% in SCCs and AKs, respectively (Table S4). *PPARG* expression was reduced by 58.3% in SCCs and 50.5% in AKs (Table S4). Finally, *PPARD* expression was increased by 2.83-fold in SCCs and 2.48-fold in AKs (Table S4). Thus, these data suggest that alterations in PPAR expression are likely observed in tumor cells themselves. Whether a similar alteration in expression occurs within stromal cells is unclear and requires additional studies.

Since *PPAR* expression at the transcript level does not necessarily imply PPAR activity, we next performed an upstream regulator analysis via IPA to determine whether alterations in PPAR isoform activity occur in NMSC. In Figure 5E, we plot the predicted mean activation z-scores for PPARα, PPARδ, and PPARγ for the tumor datasets. In SES relative to NES, the mean z-scores for all three PPARs were not significantly different from zero, indicating that none of the PPARs are predicted to be activated or inhibited in normal chronically sun-damaged skin. In contrast, a trend towards decreased PPARα and PPARγ z-scores is seen in AK lesions, while significantly negative z-scores are observed in human SCCs and BCCs and mouse SCCs. In the cases of all three malignancies, the mean z-scores met or exceeded the z-score cutoff of -2.0, which predicted that both PPARα and PPARγ signaling are inhibited and correlate well with the expression data observed in Figure 5D.

While the predicted activity for both PPARα and PPARγ match up well with the expression data, the activity score for PPARδ in Figure 5E is the opposite of what would be predicted simply by assessing *PPARD* expression in Figure 5D. This is particularly notable for the mouse SCCs in which *PPARD* expression is significantly elevated, while PPARδ activity is predicted to be inhibited. The discordant results between *PPARD* expression

and PPARδ activity could potentially be explained by reduced RXRα activity. Thus, the inhibition of the RXR function, such as through LPS or IL1 signaling, could indirectly suppress all RXRα heterodimeric partners, including PPARδ. The idea that all heterotrimeric partners of RXRα might be inhibited is supported by a shift from increased "LXR/RXR Activity" canonical pathway z-scores in sun-damaged skin to a reduction in "LXR/RXR Activity" z-scores for AKs, BCCs, and human and mouse SCCs (Figure S5).

Finally, conflicting data are seen in BCCs. Figure 5A,B indicate that PPAR signaling overall and PPARα/RXRα activation are not significantly altered in BCCs. Yet, like AKs and SCCs, *PPARA* and *PPARG* expression are decreased in Figure 5D, and the activity of all three PPARs are predicted to be inhibited in Figure 5E. While it is difficult to explain these discrepant results, it is possible that the differential epigenetic regulation of PPAR-specific target genes in neoplastic basal cell populations results in a skewed analysis of PPAR activity.

3.7. Increased PPARD Expression Represents a Marker of Myofibroblast Populations Found in Pparg-/-^epi Skin

Given that the loss of PPAR signaling and *PPAR* expression is a feature of AKs and SCCs, we examined the expression of the three PPAR isoforms within the individual cell clusters of our scRNAseq dataset. In Figure 6A,B, *Ppara* and *Pparg* are highly expressed only within the small sebocyte cluster (cluster 19). This is not surprising as PPARα and PPARγ are key to the lipogenesis that is needed to produce the sebum present in mature sebocytes [37]. The importance of PPARγ in sebocyte differentiation is seen in the absence of lipid-filled sebocytes in the dermis of *Pparg-/-*^epi mice [6]. It is therefore not surprising that all of the sebocytes that were identified in the scRNAseq unsupervised cell clustering were found in the WT mice (Table S3).
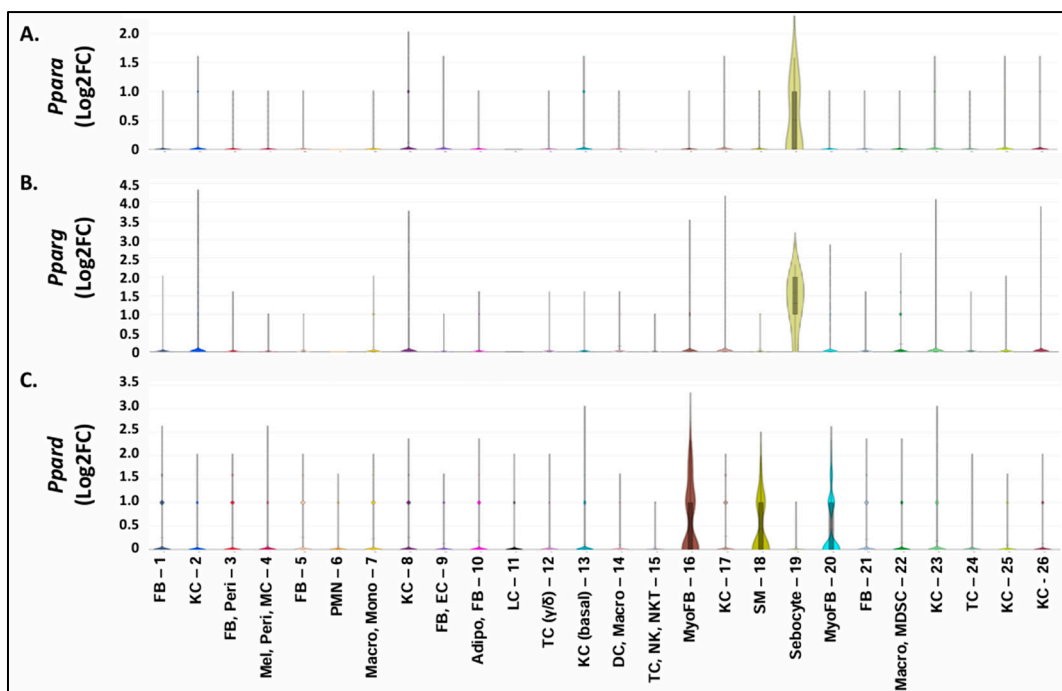

Figure 6. Cell clusters with a high level of expression of the three PPAR isoforms. (**A–C**) The expressions of *Ppara* (**A**), *Pparg* (**B**), and *Ppard* (**C**) are shown for all of the individual cell clusters obtained following the scRNAseq of skin cells (combined cells isolated from both WT and *Pparg-/-*^epi mouse skin). Both *Ppara* and *Pparg* expression were highly enriched in sebocyte cluster 19. In contrast, *Ppard* expression was enriched in myofibroblasts (clusters 16 and 20) and smooth muscle cells (cluster 18).

In contrast to *Ppara* and *Pparg*, *Ppard* was highly expressed only in the fibroblast clusters with myofibroblast features as well as the smooth muscle cell cluster (Figure 6C). This is somewhat surprising and suggests that high *Ppard* expression in mouse fibroblasts may represent a marker of myofibroblast differentiation. It might be noted that myofibroblasts are increased in the tumor microenvironment [38]. Thus, future studies are needed to determine whether cancer-associated fibroblasts with myofibroblast features also overexpress *Ppard*. As noted above, laser capture microdissection data of human AKs and SCCs indicate that increased *PPARD* occurs within the tumor cells themselves (Table S4 and [36]). Thus, it remains to be seen whether tumor-associated myofibroblasts may be contributing to the increase in *PPARD* mRNA that was observed in the NMSCs. If so, studies to determine the role of PPARδ in cancer-associated fibroblast formation and function would be of interest.

Unfortunately, scRNAseq lacks the sensitivity to assess the level of PPAR isoform transcripts in the remaining clusters seen in Figure 6A–C. Thus, the absence of measurable *Pparg* expression in cluster 10 is surprising. The Enrichr analysis indicated that the gene expression signature of cluster 10 cells aligned with both fibroblasts and adipocytes. PPARγ expression is well known to be markedly upregulated during adipocyte differentiation and is necessary for adipogenesis [39]. The absence of increased *Pparg* expression in this cluster indicates that differentiated adipocytes were not present. This suggests that the adipocyte features in this cluster are reflective of the presence of adipocyte progenitor cells [40] or adipocyte-derived fibroblasts [41]. It should also be noted that the absence of mature adipocytes was also by design, as our cell isolation methodology included low-speed centrifugation to remove less dense lipid-laden adipocytes from our collection. This allowed us to enhance the overall cell viability as well as to enrich our cell population for stromal fibroblasts and immune cells.

4. Discussion

In this report, we show that the loss of epidermal *Pparg* in mice is sufficient to induce transcriptomic changes that mimic those observed in actinic disease and SCCs. These changes include multiple changes in inflammatory signaling, chemokine expression, and immune cell recruitment. The gene set enrichment analysis revealed largely similar activation and inhibition profiles for canonical signaling pathways and diseases and biofunctions. A surprising and informative finding is that there was a switch from increased PPAR signaling in normal sun-exposed skin (SES) to a loss of PPAR signaling in AKs and cutaneous SCCs. This PPAR signaling switch correlates with a similar switch between increased *PPARG* expression in SES to reduced *PPARG* expression in malignant AK and cutaneous SCC lesions. A similar but less intense change in the pattern of *PPARA* expression was also observed. In contrast, *PPARD* expression was increased in both AKs and cutaneous SCCs. This indicates that the loss of overall PPAR signaling and an associated loss of *PPARG* and *PPARA* expression are important features that distinguish NMSC from sun-damaged skin. To our knowledge, this report is the first to demonstrate that PPAR signaling is the top commonly inhibited canonical signaling pathway in SCC development. We and others have shown that the loss of epidermal *Pparg* promotes both chemical and photocarcinogenesis in mice [9,11,12]. Thus, our data further support the idea that PPARγ acts as a potential tumor suppressor in both human and murine cutaneous SCC formation.

There are multiple potential mechanisms through which PPARγ activity could be lost in cutaneous neoplasia. These include genetic deletions or inactivating mutations. Since the germline loss of one *Pparg* allele in mice results in an increased susceptibility to chemical carcinogenesis [12], the complete loss of PPARγ activity is likely not necessary for increased tumorigenesis. The human *PPARG* gene is located at the 3p25 chromosomal locus [42]. It is therefore of interest that the loss of heterozygosity (LOH) of large portions of 3p was observed in 25% of AKs and 53% of cutaneous SCCs [43]. Another study showed that the chromosomal loss of 3p was seen in 53% of SCCs and 60% of SCCs in situ [44]. The LOH for 3p has also been described in two of five human SCC cell lines (SCC-12 and MET-1, but not SCC-13, SCL-I, or SCL-II) [45]. In addition, the LOH of chromosomal locus 3p25 is common

in related head and neck SCCs (54%) [46] and laryngeal SCCs (60%) [47]. Interestingly, the LOH of 3p25 was not seen in any of the 10 cases of non-malignant laryngeal squamous metaplasia [47]. As we found that *PPARG* expression was not reduced in sun-exposed skin, this supports the idea that the loss of PPARγ expression and activity is a tumor-specific event. In contrast to *PPARG*, the LOH at chromosomal loci for the *PPARA* gene (22q) or the *PPARD* gene (6p) is infrequent (<5%) in cutaneous SCCs [43,45,48,49].

Loss-of-function somatic missense mutations of *PPARG* have also been described in cancer but are not particularly common [50]. However, as UV is a potent mutagen and UV-induced tumors have the highest reported mutation burden of human cancers [51], it is possible that somatic LOF mutations are more frequent in cutaneous SCCs.

An additional potential mechanism for the loss of PPARγ signaling in AK and SCCs includes alternative splice variants with dominant negative (dnPPARγ) activity. A number of dnPPARγ splice variants have been shown to be increased in cancer (γORF4 [52], hPPARγ1$_{tr}$ [53], and PPARγΔ5 [54]). In mice, both TNF and LPS suppress *Pparg* expression and induce *Pparg*Δ5 splice variant expression, providing a mechanism for the loss of PPARγ activity through alternative splicing [33]. In the case of hPPARγ1$_{tr}$, the expression of this splice variant was identified in lung SCCs but not adjacent normal tissue [53]. Thus, the upregulation of dnPPARγ variants, specifically in tumors, could also account for reduced PPARγ activity.

Reduced *PPARG* and *PPARA* expression have also been documented in some cancers through micro RNAs (miRNAs), long non-coding RNAs (lncRNAs), and promoter hypermethylation.

Using Targetscan 8.0 [55,56], 274 or 502 distinct miRNAs are predicted to target human *PPARG* or mouse *Pparg*, respectively. While the role of miRNAs in suppressing *PPARG* expression has not been adequately studied in NMSC, one study demonstrated that miR-27b, miR-130b, and miR-138 are all upregulated in colon cancer and correlate negatively with *PPARG* mRNA and protein expression [57]. In addition, the elevation of miR-374a/-128/-130b was seen in seven cases of human cutaneous SCCs relative to non-lesional skin [58]. All three of these miRNAs are predicted to bind to the human PPARG 3′-UTR, although a role in regulating *PPARG* expression was not addressed.

Like miRNAs, a number of lncRNAs have the ability to alter PPAR expression [59]. MALAT1 is a known lncRNA regulator of tumor development and is overexpressed in cutaneous SCCs [60,61]. MALAT1 is also thought to target *PPARG* [59]. In competing endogenous RNA networks (ceRNA networks), sequence homology between lncRNAs and miRNAs competes for miRNA target binding to suppress the regulatory function of miRNAs. A study of human cutaneous SCCs examined correlations between 3221 differentially expressed transcripts and 24 differentially expressed lncRNAs (DElncRNA). By incorporating known miRNA targets of the lncRNAs, they were able to predict ceRNA networks that are operational in cutaneous SCCs [62]. Of the 24 DElncRNAs that were identified, 5 were predicted to target *PPARG* (HCG18, LINC00342, HLA-F-AS1, SNX29P2, and POLR214) [62]. In addition, all five were downregulated. Thus, the loss of these lncRNAs could, in turn, promote the miRNA-induced suppression of *PPARG* expression. Consistent with this idea, *PPARG* expression was decreased in their dataset (Log2FC of −0.91071; FDR 1.73×10^{-7}).

Another epigenetic mechanism for the potential loss of *PPARG* expression in skin cancer is promoter hypermethylation. Promoter hypermethylation of the *PPARG* gene by ubiquitin-like, containing PHD and RING finger domains, 1 (UHRF1) are associated with poor prognosis in colorectal cancer [63]. However, it has yet to be determined whether promoter methylation and the silencing of *PPARG* gene expression occur in NMSC.

Finally, recent studies indicate that PPARγ and NF-κB signaling have a complex and mutually antagonistic relationship. Studies in adipocytes, mesenchymal stem cells, and macrophages show that stimulation with LPS or TNFα act to suppress overall *PPARG/Pparg* transcript expression and target gene expression [33]. The constitutive activation of NF-κB has been described as a common feature of malignancy due to activating mutations of

NF-κB transcription factors themselves or upstream regulators [64]. It is possible that the loss of *PPARG* expression or activity through any of these epigenetic or genetic mechanisms could result in a self-sustaining negative feedback cycle whereby the initial loss of PPARγ anti-inflammatory activity results in increased inflammatory cytokine production that results in a further degradation of PPARγ signaling within the tumor cells themselves or surrounding stromal cells.

The decrease in PPARα expression suggests that this transcription factor may also play a tumor suppressor role, particularly in mouse SCCs. Further studies are needed to clarify the degree to which PPARγ and PPARα activity are suppressed in NMSC and the mechanisms through which this occurs. It would therefore be of interest to determine the degree to which mice lacking epidermal *Ppara* exhibit transcriptomic changes that mirror those observed in AKs, SCCs, and *Pparg-/-*-epi mice.

Given that PPARγ has an important anti-inflammatory role, it is not surprising that another key finding from our analysis is that inflammatory signaling and immune cell activation are a common feature of *Pparg-/-*-epi mice, Aks, and SCCs. This suggests that the loss of PPARγ activity acts to promote neoplasia through its ability to induce stromal changes associated with tumorigenesis. This included a prominent accumulation of neutrophils and macrophage cells. It might be noted that mice expressing dominant negative *Pparg* (dn*Pparg*) in type II pulmonary alveolar cells stimulate the mobilization and recruitment of myeloid cells with MDSC activity [65]. Given that *Pparg-/-*-epi mice have a marked defect in CHS responses, it is tempting to speculate that the myeloid cell infiltrate that we observe exhibits MDSC activity. However, additional functional studies are needed to verify whether these myeloid cells represent MDSCs and contribute to the immune suppression seen in *Pparg-/-*-epi mice.

An interesting feature of our analysis is the increase in *PPARD/Ppard* during malignant progression. It is possible that whatever mechanism is involved in downregulating PPARγ and PPARα expression fails to elicit the downregulation of PPARδ. Alternatively, since PPAR isoforms have overlapping functions, particularly in cellular energy production [66], the increase in *PPARD/Ppard* may also serve a compensatory function to mitigate the changes that are caused by a loss of the other isoforms in human and mouse tumors. The increase in PPARδ may also promote tumor angiogenesis and progression through its effects on endothelial cells [67].

Another potential explanation for the increase in PPARδ transcripts in AKs and SCCs might be implied by our scRNAseq data from *Pparg-/-*-epi mice. We found that *Ppard* expression was increased in *Pparg-/-*-epi mice, particularly in fibroblasts expressing myofibroblast markers. It has been reported that PPARδ mediates fibroblast differentiation to profibrotic myofibroblasts by inducing the expression of TGFβ, which, in turn, induces the expression of alpha smooth muscle actin [68]. While the significance of this finding requires further studies, the presence of myofibroblasts is associated with chronic inflammation, fibrosis, and wound healing [69]. Myofibroblast markers are also associated with cancer-associated fibroblasts (CAFs) [70]. Thus, the observed increase in *PPARD/Ppard* expression in the tumor datasets may simply reflect an increase in myofibroblasts that are characteristic of the tumor stroma. Moreover, as PPARγ activation suppresses TGFβ expression and myofibroblast differentiation [71], this may also indicate that PPARγ and PPARδ have opposing actions in myofibroblast differentiation and fibrosis.

A weakness of our studies is that our mouse model results in the embryonic loss of *Pparg*. Thus, our studies carried out in adult mice would cause them to suffer from long-standing dermal inflammatory changes that would create a new normal homeostatic state. Thus, the proximal events that are first initiated by the loss of epidermal PPARγ cannot be assessed. If the loss of *PPARG* is a defining feature of NMSC tumor–stroma interactions, then it would be important to determine the nature of these early signals to identify potential interventional targets. While this would be difficult to achieve in our *Pparg-/-*-epi mice, these studies could be performed in floxed *Pparg* mice crossed with a tamoxifen-inducible Krt14-Cre transgene.

In conclusion, the loss of PPARγ expression and activity is a top feature of both *Pparg-/-*^{epi} mouse skin and AK and SCC transcriptomic datasets. A more modest reduction in PPARα expression and activity is also observed. A single-cell analysis also reveals that *Pparg-/-*^{epi} mouse skin exhibits immune cell infiltrates and myofibroblast differentiation that is indicative of a chronic inflammatory state. This genomic approach supports previous studies indicating that PPARγ is an important tumor suppressor in cutaneous carcinogenesis, leading to actinic disease and squamous cell carcinoma. Specifically, the loss of tumor cell-specific PPARγ activity may be necessary for the establishment of the stromal inflammatory microenvironment that is a hallmark of neoplastic disease in the skin.

Supplementary Materials: The following supporting information can be downloaded at https://www.mdpi.com/article/10.3390/cells13161356/s1, Figure S1: Single-cell RNA sequencing data summary for wildtype (WT) mouse skin. Figure S2: Single-cell RNA sequencing data summary for *Pparg-/-*^{epi} (KO) mouse skin. Figure S3: Top diseases and biofunctions that are common in *Pparg-/-*^{epi} mice and human BCCs. Figure S4: Top canonical pathways that are common in *Pparg-/-*^{epi} mice and human BCCs. Figure S5: Canonical pathway analysis showing tumor-specific reduction in LXR/RXR activation. Table S1: Full list of diseases and biofunctions that annotate to *Pparg-/-*^{epi} mouse skin DEG dataset. Table S2: Full list of DEGs from single-cell RNA sequencing. Table S3: Cluster identification. Table S4: Published transcriptomic datasets used for analysis. References [28,34–36,72–90] are cited in Supplementary Materials.

Author Contributions: Conceptualization, R.L.K.; methodology, R.L.K., X.X., E.D.-Y. and F.F.; software, R.L.K. and H.G.; formal analysis, R.L.K.; writing—original draft preparation, R.L.K.; writing—review and editing, R.L.K.; supervision, R.L.K. and Y.L.; project administration, R.L.K.; funding acquisition, R.L.K. All authors have read and agreed to the published version of the manuscript.

Institutional Review Board Statement: The animal study protocol was approved by the Institutional Review Board (Institutional Animal Care and Use Committee) of the Indiana University School of Medicine and the Richard L. Roudebush VA Medical Center (protocol 11256, approved on 19 April 2017, and protocol 20006, approved on 3 November 2020).

Informed Consent Statement: Not applicable.

Data Availability Statement: The raw data supporting the conclusions of this article will be made available by the corresponding author upon request. Some of the data in this report were derived from resources available in the public domain [see Table S4 for public dataset sources].

Conflicts of Interest: The authors declare no conflicts of interest. The funders had no role in the design of the study; in the collection, analyses, or interpretation of data; in the writing of the manuscript; or in the decision to publish the results.

References

1. Germain, P.; Staels, B.; Dacquet, C.; Spedding, M.; Laudet, V. Overview of Nomenclature of Nuclear Receptors. *Pharmacol. Rev.* **2006**, *58*, 685–704. [CrossRef] [PubMed]
2. Pirat, C.; Farce, A.; Lebègue, N.; Renault, N.; Furman, C.; Millet, R.; Yous, S.; Speca, S.; Berthelot, P.; Desreumaux, P.; et al. Targeting Peroxisome Proliferator-Activated Receptors (PPARs): Development of Modulators. *J. Med. Chem.* **2012**, *55*, 4027–4061. [CrossRef] [PubMed]
3. Wagner, K.D.; Wagner, N. Peroxisome proliferator-activated receptor beta/delta (PPARβ/δ) acts as regulator of metabolism linked to multiple cellular functions. *Pharmacol. Ther.* **2010**, *125*, 423–435. [CrossRef] [PubMed]
4. Schmuth, M.; Moosbrugger-Martinz, V.; Blunder, S.; Dubrac, S. Role of PPAR, LXR, and PXR in epidermal homeostasis and inflammation. *Biochim. Biophys. Acta-Mol. Cell Biol. Lipids* **2014**, *1841*, 463–473. [CrossRef] [PubMed]
5. Pascual, G.; Fong, A.L.; Ogawa, S.; Gamliel, A.; Li, A.C.; Perissi, V.; Rose, D.W.; Willson, T.M.; Rosenfeld, M.G.; Glass, C.K. A SUMOylation-dependent pathway mediates transrepression of inflammatory response genes by PPAR-γ. *Nature* **2005**, *437*, 759–763. [CrossRef] [PubMed]

6. Konger, R.L.; Derr-Yellin, E.; Zimmers, T.A.; Katona, T.; Xuei, X.; Liu, Y.; Zhou, H.-M.; Simpson, E.R.; Turner, M.J. Epidermal PPARγ Is a Key Homeostatic Regulator of Cutaneous Inflammation and Barrier Function in Mouse Skin. *Int. J. Mol. Sci.* **2021**, *22*, 8634. [CrossRef]

7. Mahgoub, D.; El Tawdy, A.M.; Metwally, D.; Manar, A.; Rashed, L. Estimation of peroxisomal proliferators-activated receptor γ gene expression in inflammatory skin diseases: Atopic dermatitis and psoriasis. *Our Dermatol. Online* **2014**, *5*, 107–112. [CrossRef]

8. Karnik, P.; Tekeste, Z.; McCormick, T.S.; Gilliam, A.C.; Price, V.H.; Cooper, K.D.; Mirmirani, P. Hair Follicle Stem Cell-Specific PPARγ Deletion Causes Scarring Alopecia. *J. Investig. Dermatol.* **2008**, *129*, 1243–1257. [CrossRef]

9. Sahu, R.P.; DaSilva, S.C.; Rashid, B.; Martel, K.C.; Jernigan, D.; Mehta, S.R.; Mohamed, D.R.; Rezania, S.; Bradish, J.R.; Armstrong, A.B.; et al. Mice lacking epidermal PPARγ exhibit a marked augmentation in photocarcinogenesis associated with increased UVB-induced apoptosis, inflammation and barrier dysfunction. *Int. J. Cancer* **2012**, *131*, E1055–E1066. [CrossRef]

10. Konger, R.L.; Derr-Yellin, E.; Travers, J.B.; Ocana, J.A.; Sahu, R.P. Epidermal PPARγ influences subcutaneous tumor growth and acts through TNF-α to regulate contact hypersensitivity and the acute photoresponse. *Oncotarget* **2017**, *8*, 98184–98199. [CrossRef]

11. Indra, A.K.; Castaneda, E.; Antal, M.C.; Jiang, M.; Messaddeq, N.; Meng, X.; Loehr, C.V.; Gariglio, P.; Kato, S.; Wahli, W.; et al. Malignant transformation of DMBA/TPA-induced papillomas and nevi in the skin of mice selectively lacking retinoid-X-receptor α in epidermal keratinocytes. *J. Investig. Dermatol.* **2007**, *127*, 1250–1260. [CrossRef] [PubMed]

12. Nicol, C.J.; Yoon, M.; Ward, J.M.; Yamashita, M.; Fukamachi, K.; Peters, J.M.; Gonzalez, F.J. PPARgamma influences susceptibility to DMBA-induced mammary, ovarian and skin carcinogenesis. *Carcinogenesis* **2004**, *25*, 1747–1755. [CrossRef] [PubMed]

13. Ren, L.; Konger, R.L. Evidence that peroxisome proliferator-activated receptor γ suppresses squamous carcinogenesis through anti-inflammatory signaling and regulation of the immune response. *Mol. Carcinog.* **2019**, *58*, 1589–1601. [CrossRef] [PubMed]

14. Konger, R.L.; Derr-Yellin, E.; Ermatov, N.; Ren, L.; Sahu, R.P. The PPARγ Agonist Rosiglitazone Suppresses Syngeneic Mouse SCC (Squamous Cell Carcinoma) Tumor Growth through an Immune-Mediated Mechanism. *Molecules* **2019**, *24*, 2192. [CrossRef] [PubMed]

15. Goyal, G.; Wong, K.; Nirschl, C.J.; Souders, N.; Neuberg, D.; Anandasabapathy, N.; Dranoff, G. PPARγ Contributes to Immunity Induced by Cancer Cell Vaccines That Secrete GM-CSF. *Cancer Immunol. Res.* **2018**, *6*, 723–732. [CrossRef] [PubMed]

16. Ritter, B.; Greten, F.R. Modulating inflammation for cancer therapy. *J. Exp. Med.* **2019**, *216*, 1234–1243. [CrossRef] [PubMed]

17. Thorsson, V.; Gibbs, D.L.; Brown, S.D.; Wolf, D.; Bortone, D.S.; Ou Yang, T.-H.; Porta-Pardo, E.; Gao, G.F.; Plaisier, C.L.; Eddy, J.A.; et al. The Immune Landscape of Cancer. *Immunity* **2018**, *48*, 812–830.e14. [CrossRef] [PubMed]

18. Young, M.D.; Behjati, S. SoupX removes ambient RNA contamination from droplet-based single-cell RNA sequencing data. *Gigascience* **2020**, *9*, giaa151. [CrossRef]

19. Satija, R.; Farrell, J.A.; Gennert, D.; Schier, A.F.; Regev, A. Spatial reconstruction of single-cell gene expression data. *Nat. Biotechnol.* **2015**, *33*, 495–502. [CrossRef]

20. Butler, A.; Hoffman, P.; Smibert, P.; Papalexi, E.; Satija, R. Integrating single-cell transcriptomic data across different conditions, technologies, and species. *Nat. Biotechnol.* **2018**, *36*, 411–420. [CrossRef]

21. Stuart, T.; Butler, A.; Hoffman, P.; Hafemeister, C.; Papalexi, E.; Mauck, W.M., III; Hao, Y.; Stoeckius, M.; Smibert, P.; Satija, R. Comprehensive Integration of Single-Cell Data. *Cell* **2019**, *177*, 1888–1902.e21. [CrossRef]

22. Hao, Y.; Hao, S.; Andersen-Nissen, E.; Mauck, W.M., III; Zheng, S.; Butler, A.; Lee, M.J.; Wilk, A.J.; Darby, C.; Zager, M.; et al. Integrated analysis of multimodal single-cell data. *Cell* **2021**, *184*, 3573–3587.e29. [CrossRef] [PubMed]

23. McCarthy, D.J.; Campbell, K.R.; Lun, A.T.; Wills, Q.F. Scater: Pre-processing, quality control, normalization and visualization of single-cell RNA-seq data in R. *Bioinformatics* **2017**, *33*, 1179–1186. [CrossRef] [PubMed]

24. Chen, E.Y.; Tan, C.M.; Kou, Y.; Duan, Q.; Wang, Z.; Meirelles, G.V.; Clark, N.R.; Ma'ayan, A. Enrichr: Interactive and collaborative HTML5 gene list enrichment analysis tool. *BMC Bioinform.* **2013**, *14*, 128. [CrossRef]

25. Kuleshov, M.V.; Jones, M.R.; Rouillard, A.D.; Fernandez, N.F.; Duan, Q.; Wang, Z.; Koplev, S.; Jenkins, S.L.; Jagodnik, K.M.; Lachmann, A.; et al. Enrichr: A comprehensive gene set enrichment analysis web server 2016 update. *Nucleic Acids Res.* **2016**, *44*, W90–W97. [CrossRef]

26. Xie, Z.; Bailey, A.; Kuleshov, M.V.; Clarke, D.J.B.; Evangelista, J.E.; Jenkins, S.L.; Lachmann, A.; Wojciechowicz, M.L.; Kropiwnicki, E.; Jagodnik, K.M.; et al. Gene Set Knowledge Discovery with Enrichr. *Curr. Protoc.* **2021**, *1*, e90. [CrossRef] [PubMed]

27. Franzén, O.; Gan, L.-M.; Björkegren, J.L.M. PanglaoDB: A web server for exploration of mouse and human single-cell RNA sequencing data. *Database* **2019**, *2019*, baz046. [CrossRef]

28. Li, Y.; Andrade, J. DEApp: An interactive web interface for differential expression analysis of next generation sequence data. *Source Code Biol. Med.* **2017**, *12*, 2. [CrossRef]

29. Krämer, A.; Green, J.; Pollard, J., Jr.; Tugendreich, S. Causal analysis approaches in Ingenuity Pathway Analysis. *Bioinformatics* **2014**, *30*, 523–530. [CrossRef]

30. Qie, C.; Jiang, J.; Liu, W.; Hu, X.; Chen, W.; Xie, X.; Liu, J. Single-cell RNA-Seq reveals the transcriptional landscape and heterogeneity of skin macrophages in Vsir$^{-/-}$ murine psoriasis. *Theranostics* **2020**, *10*, 10483–10497. [CrossRef]

31. Apte, M.V.; Pirola, R.C.; Wilson, J.S. Pancreatic stellate cells: A starring role in normal and diseased pancreas. *Front. Physiol.* **2012**, *3*, 344. [CrossRef]

32. McAndrews, K.M.; Miyake, T.; Ehsanipour, E.A.; Kelly, P.J.; Becker, L.M.; McGrail, D.J.; Sugimoto, H.; LeBleu, V.S.; Ge, Y.; Kalluri, R. Dermal αSMA$^+$ myofibroblasts orchestrate skin wound repair via β1 integrin and independent of type I collagen production. *EMBO J.* **2022**, *41*, e109470. [CrossRef]

33. Cataldi, S.; Aprile, M.; Melillo, D.; Mucel, I.; Giorgetti-Peraldi, S.; Cormont, M.; Italiani, P.; Blüher, M.; Tanti, J.F.; Ciccodicola, A.; et al. TNFα Mediates Inflammation-Induced Effects on PPARG Splicing in Adipose Tissue and Mesenchymal Precursor Cells. *Cells* **2021**, *11*, 42. [CrossRef]

34. Kita, R.; Fraser, H.B. Local Adaptation of Sun-Exposure-Dependent Gene Expression Regulation in Human Skin. *PLoS Genet.* **2016**, *12*, e1006382. [CrossRef]

35. Zou, D.-D.; Xu, D.; Deng, Y.-Y.; Wu, W.-J.; Zhang, J.; Huang, L.; He, L. Identification of key genes in cutaneous squamous cell carcinoma: A transcriptome sequencing and bioinformatics profiling study. *Ann. Transl. Med.* **2021**, *9*, 1497. [CrossRef] [PubMed]

36. Mitsui, H.; Suárez-Fariñas, M.; Gulati, N.; Shah, K.R.; Cannizzaro, M.V.; Coats, I.; Felsen, D.; Krueger, J.G.; Carucci, J.A. Gene expression profiling of the leading edge of cutaneous squamous cell carcinoma: IL-24-driven MMP-7. *J. Investig. Dermatol.* **2014**, *134*, 1418–1427. [CrossRef]

37. Downie, M.M.; Sanders, D.A.; Maier, L.M.; Stock, D.M.; Kealey, T. Peroxisome proliferator-activated receptor and farnesoid X receptor ligands differentially regulate sebaceous differentiation in human sebaceous gland organ cultures in vitro. *Br. J. Dermatol.* **2004**, *151*, 766–775. [CrossRef] [PubMed]

38. Butti, R.; Nimma, R.; Kundu, G.; Bulbule, A.; Kumar, T.V.S.; Gunasekaran, V.P.; Tomar, D.; Kumar, D.; Mane, A.; Gill, S.S.; et al. Tumor-derived osteopontin drives the resident fibroblast to myofibroblast differentiation through Twist1 to promote breast cancer progression. *Oncogene* **2021**, *40*, 2002–2017. [CrossRef]

39. Hansson, B.; Rippe, C.; Kotowska, D.; Wasserstrom, S.; Säll, J.; Göransson, O.; Swärd, K.; Stenkula, K. Rosiglitazone drives cavin-2/SDPR expression in adipocytes in a CEBPα-dependent manner. *PLoS ONE* **2017**, *12*, e0173412. [CrossRef] [PubMed]

40. Cawthorn, W.P.; Scheller, E.L.; MacDougald, O.A. Adipose tissue stem cells meet preadipocyte commitment: Going back to the future. *J. Lipid Res.* **2012**, *53*, 227–246. [CrossRef]

41. Bochet, L.; Lehuédé, C.; Dauvillier, S.; Wang, Y.Y.; Dirat, B.; Laurent, V.; Dray, C.; Guiet, R.; Maridonneau-Parini, I.; Le Gonidec, S.; et al. Adipocyte-Derived Fibroblasts Promote Tumor Progression and Contribute to the Desmoplastic Reaction in Breast Cancer. *Cancer Res.* **2013**, *73*, 5657–5668. [CrossRef] [PubMed]

42. Costa-Guda, J.; Rosen, E.D.; Jensen, R.T.; Chung, D.C.; Arnold, A. Mutational analysis of PPARG as a candidate tumour suppressor gene in enteropancreatic endocrine tumours. *Clin. Endocrinol.* **2005**, *62*, 603–606. [CrossRef] [PubMed]

43. Ashton, K.J.; Weinstein, S.R.; Maguire, D.J.; Griffiths, L.R. Chromosomal Aberrations in Squamous Cell Carcinoma and Solar Keratoses Revealed by Comparative Genomic Hybridization. *Arch. Dermatol.* **2003**, *139*, 876–882. [CrossRef]

44. Ashton, K.J.; Carless, M.A.; Griffiths, L.R. Cytogenetic alterations in nonmelanoma skin cancer: A review. *Genes Chromosomes Cancer* **2005**, *43*, 239–248. [CrossRef]

45. Popp, S.; Waltering, S.; Herbst, C.; Moll, I.; Boukamp, P. UV-B-type mutations and chromosomal imbalances indicate common pathways for the development of Merkel and skin squamous cell carcinomas. *Int. J. Cancer* **2002**, *99*, 352–360. [CrossRef]

46. Maestro, R.; Gasparotto, D.; Vukosavljevic, T.; Barzan, L.; Sulfaro, S.; Boiocchi, M. Three Discrete Regions of Deletion at 3p in Head and Neck Cancers. *Cancer Res.* **1993**, *53*, 5775–5779. [PubMed]

47. Yoo, W.J.; Cho, S.H.; Lee, Y.S.; Park, G.S.; Kim, M.S.; Kim, B.K.; Park, W.S.; Lee, J.Y.; Kang, C.S. Loss of heterozygosity on chromosomes 3p,8p,9p and 17p in the progression of squamous cell carcinoma of the larynx. *J. Korean Med. Sci.* **2004**, *19*, 345–351. [CrossRef]

48. Rehman, I.; Takata, M.; Wu, Y.Y.; Rees, J.L. Genetic change in actinic keratoses. *Oncogene* **1996**, *12*, 2483–2490.

49. Quinn, A.G.; Sikkink, S.; Rees, J.L. Basal Cell Carcinomas and Squamous Cell Carcinomas of Human Skin Show Distinct Patterns of Chromosome Loss. *Cancer Res.* **1994**, *54*, 4756–4759.

50. Ikezoe, T.; Miller, C.W.; Kawano, S.; Heaney, A.; Williamson, E.A.; Hisatake, J.; Green, E.; Hofmann, W.; Taguchi, H.; Koeffler, H.P. Mutational analysis of the peroxisome proliferator-activated receptor gamma gene in human malignancies. *Cancer Res.* **2001**, *61*, 5307–5310.

51. Chalmers, Z.R.; Connelly, C.F.; Fabrizio, D.; Gay, L.; Ali, S.M.; Ennis, R.; Schrock, A.; Campbell, B.; Shlien, A.; Chmielecki, J.; et al. Analysis of 100,000 human cancer genomes reveals the landscape of tumor mutational burden. *Genome Med.* **2017**, *9*, 34. [CrossRef]

52. Aprile, M.; Ambrosio, M.R.; D'Esposito, V.; Beguinot, F.; Formisano, P.; Costa, V.; Ciccodicola, A. PPARG in Human Adipogenesis: Differential Contribution of Canonical Transcripts and Dominant Negative Isoforms. *PPAR Res.* **2014**, *2014*, 537865. [CrossRef] [PubMed]

53. Kim, H.J.; Hwang, J.Y.; Kim, H.J.; Choi, W.S.; Lee, J.H.; Kim, H.J.; Chang, K.C.; Nishinaka, T.; Yabe-Nishimura, C.; Seo, H.G. Expression of a peroxisome proliferator-activated receptor gamma 1 splice variant that was identified in human lung cancers suppresses cell death induced by cisplatin and oxidative stress. *Clin. Cancer Res.* **2007**, *13*, 2577–2583. [CrossRef]

54. Hernandez-Quiles, M.; Broekema, M.F.; Kalkhoven, E. PPARgamma in Metabolism, Immunity, and Cancer: Unified and Diverse Mechanisms of Action. *Front. Endocrinol.* **2021**, *12*, 624112. [CrossRef] [PubMed]

55. McGeary, S.E.; Lin, K.S.; Shi, C.Y.; Pham, T.M.; Bisaria, N.; Kelley, G.M.; Bartel, D.P. The biochemical basis of microRNA targeting efficacy. *Science* **2019**, *366*, eaav1741. [CrossRef]

56. Agarwal, V.; Bell, G.W.; Nam, J.-W.; Bartel, D.P. Predicting effective microRNA target sites in mammalian mRNAs. *eLife* **2015**, *4*, e05005. [CrossRef]

57. Motawi, T.K.; Shaker, O.G.; Ismail, M.F.; Sayed, N.H. Peroxisome Proliferator-Activated Receptor Gamma in Obesity and Colorectal Cancer: The Role of Epigenetics. *Sci. Rep.* **2017**, *7*, 10714. [CrossRef] [PubMed]

58. Sand, M.; Skrygan, M.; Georgas, D.; Sand, D.; Hahn, S.A.; Gambichler, T.; Altmeyer, P.; Bechara, F.G. Microarray analysis of microRNA expression in cutaneous squamous cell carcinoma. *J. Dermatol. Sci.* **2012**, *68*, 119–126. [CrossRef]

59. Kazeminasab, F.; Baharlooie, M.; Ghaedi, K. Noncoding RNAs Associated with PPARs in Etiology of MAFLD as a Novel Approach for Therapeutics Targets. *PPAR Res.* **2022**, *2022*, 6161694. [CrossRef]

60. Li, S.-S.; Zhou, L.; Gao, L.; Wang, Y.-H.; Ding, Z.-H. Role of long noncoding RNA MALAT1 promotes the occurrence and progression of cutaneous squamous cell carcinoma. *Nan Fang Yi Ke Da Xue Xue Bao* **2018**, *38*, 421–427. [CrossRef]

61. Zhang, C.; Wang, J.; Guo, L.; Peng, M. Long non-coding RNA MALAT1 regulates cell proliferation, invasion and apoptosis by modulating the Wnt signaling pathway in squamous cell carcinoma. *Am. J. Transl. Res.* **2021**, *13*, 9233–9240.

62. Xu, Y.; Dong, Y.; Deng, Y.; Qi, Q.; Wu, M.; Liang, H.; She, Q.; Guo, Q. Identifying an lncRNA-Related ceRNA Network to Reveal Novel Targets for a Cutaneous Squamous Cell Carcinoma. *Biology* **2021**, *10*, 432. [CrossRef] [PubMed]

63. Sabatino, L.; Fucci, A.; Pancione, M.; Carafa, V.; Nebbioso, A.; Pistore, C.; Babbio, F.; Votino, C.; Laudanna, C.; Ceccarelli, M.; et al. UHRF1 coordinates peroxisome proliferator activated receptor gamma (PPARG) epigenetic silencing and mediates colorectal cancer progression. *Oncogene* **2012**, *31*, 5061–5072. [CrossRef]

64. Gilmore, T.D. NF-κB and Human Cancer: What Have We Learned over the Past 35 Years? *Biomedicines* **2021**, *9*, 889. [CrossRef]

65. Wu, L.; Wang, G.; Qu, P.; Yan, C.; Du, H. Overexpression of Dominant Negative Peroxisome Proliferator-Activated Receptor-γ (PPARγ) in Alveolar Type II Epithelial Cells Causes Inflammation and T-Cell Suppression in the Lung. *Am. J. Pathol.* **2011**, *178*, 2191–2204. [CrossRef] [PubMed]

66. Grygiel-Górniak, B. Peroxisome proliferator-activated receptors and their ligands: Nutritional and clinical implications—A review. *Nutr. J.* **2014**, *13*, 17. [CrossRef] [PubMed]

67. Wagner, K.-D.; Du, S.; Martin, L.; Leccia, N.; Michiels, J.-F.; Wagner, N. Vascular PPARβ/δ Promotes Tumor Angiogenesis and Progression. *Cells* **2019**, *8*, 1623. [CrossRef]

68. Ham, S.A.; Hwang, J.S.; Yoo, T.; Lee, W.J.; Paek, K.S.; Oh, J.-W.; Park, C.-K.; Kim, J.-H.; Do, J.T.; Kim, J.-H.; et al. Ligand-activated PPARδ upregulates α-smooth muscle actin expression in human dermal fibroblasts: A potential role for PPARδ in wound healing. *J. Dermatol. Sci.* **2015**, *80*, 186–195. [CrossRef]

69. Tai, Y.; Woods, E.L.; Dally, J.; Kong, D.; Steadman, R.; Moseley, R.; Midgley, A.C. Myofibroblasts: Function, Formation, and Scope of Molecular Therapies for Skin Fibrosis. *Biomolecules* **2021**, *11*, 1095. [CrossRef]

70. Procopio, M.G.; Laszlo, C.; Al Labban, D.; Kim, D.E.; Bordignon, P.; Jo, S.H.; Goruppi, S.; Menietti, E.; Ostano, P.; Ala, U.; et al. Combined CSL and p53 downregulation promotes cancer-associated fibroblast activation. *Nat. Cell Biol.* **2015**, *17*, 1193–1204. [CrossRef]

71. Lecarpentier, Y.; Schussler, O.; Claes, V.; Vallée, A. The Myofibroblast: TGFβ-1, A Conductor which Plays a Key Role in Fibrosis by Regulating the Balance between PPARγ and the Canonical WNT Pathway. *Nucl. Recept. Res.* **2017**, *4*, 101299. [CrossRef] [PubMed]

72. Chitsazzadeh, V.; Coarfa, C.; Drummond, J.A.; Nguyen, T.; Joseph, A.; Chilukuri, S.; Charpiot, E.; Adelmann, C.H.; Ching, G.; Nguyen, T.N.; et al. Cross-species identification of genomic drivers of squamous cell carcinoma development across preneoplastic intermediates. *Nat. Commun.* **2016**, *7*, 12601. [CrossRef] [PubMed]

73. McCreery, M.Q.; Halliwill, K.D.; Chin, D.; Delrosario, R.; Hirst, G.; Vuong, P.; Jen, K.Y.; Hewinson, J.; Adams, D.J.; Balmain, A. Evolution of metastasis revealed by mutational landscapes of chemically induced skin cancers. *Nat. Med.* **2015**, *21*, 1514–1520. [CrossRef] [PubMed]

74. García-Escudero, R.; Martínez-Cruz, A.B.; Santos, M.; Lorz, C.; Segrelles, C.; Garaulet, G.; Saiz-Ladera, C.; Costa, C.; Buitrago-Pérez, A.; Dueñas, M.; et al. Gene expression profiling of mouse p53-deficient epidermal carcinoma defines molecular determinants of human cancer malignancy. *Mol. Cancer* **2010**, *9*, 193. [CrossRef] [PubMed]

75. Ponzio, G.; Nottet, N.; Mari, B.; Lebrigand, K.; Barbry, P.; Rezzonico, R. A new long noncoding RNA (lncRNA) is induced in cutaneous squamous cell carcinoma and down-regulates several anticancer and cell differentiation genes in mouse. *J. Biol. Chem.* **2017**, *292*, 12483–12495. [CrossRef]

76. Segura, S.; Gadea, A.; Nonell, L.; Andrades, E.; Sánchez, S.; Pujol, R.; Hernández-Muñoz, I.; Toll, A. Identification of differentially expressed genes in actinic keratosis samples treated with ingenol mebutate gel. *PLoS ONE* **2020**, *15*, e0232146. [CrossRef] [PubMed]

77. Hoang, V.L.T.; Tom, L.N.; Quek, X.-C.; Tan, J.-M.; Payne, E.J.; Lin, L.L.; Sinnya, S.; Raphael, A.P.; Lambie, D.; Frazer, I.H.; et al. RNA-seq reveals more consistent reference genes for gene expression studies in human non-melanoma skin cancers. *PeerJ* **2017**, *5*, e3631. [CrossRef] [PubMed]

78. Bailey, P.; Ridgway, R.A.; Cammareri, P.; Treanor-Taylor, M.; Bailey, U.-M.; Schoenherr, C.; Bone, M.; Schreyer, D.; Purdie, K.; Thomson, J.; et al. Driver gene combinations dictate cutaneous squamous cell carcinoma disease continuum progression. *Nat. Commun.* **2023**, *14*, 5211. [CrossRef] [PubMed]

79. Nindl, I.; Dang, C.; Forschner, T.; Kuban, R.J.; Meyer, T.; Sterry, W.; Stockfleth, E. Identification of differentially expressed genes in cutaneous squamous cell carcinoma by microarray expression profiling. *Mol. Cancer* **2006**, *5*, 30. [CrossRef]

80. Hameetman, L.; Commandeur, S.; Bavinck, J.N.; Wisgerhof, H.C.; de Gruijl, F.R.; Willemze, R.; Mullenders, L.; Tensen, C.P.; Vrieling, H. Molecular profiling of cutaneous squamous cell carcinomas and actinic keratoses from organ transplant recipients. *BMC Cancer* **2013**, *13*, 58. [CrossRef]

81. García-Díez, I.; Hernández-Muñoz, I.; Hernández-Ruiz, E.; Nonell, L.; Puigdecanet, E.; Bódalo-Torruella, M.; Andrades, E.; Pujol, R.M.; Toll, A. Transcriptome and cytogenetic profiling analysis of matched in situ/invasive cutaneous squamous cell carcinomas from immunocompetent patients. *Genes Chromosomes Cancer* **2019**, *58*, 164–174. [CrossRef] [PubMed]

82. Hu, Y.; Li, R.; Chen, H.; Chen, L.; Zhou, X.; Liu, L.; Ju, M.; Chen, K.; Huang, D. Comprehensive analysis of lncRNA-mRNAs co-expression network identifies potential lncRNA biomarkers in cutaneous squamous cell carcinoma. *BMC Genom.* **2022**, *23*, 274. [CrossRef] [PubMed]

83. Das Mahapatra, K.; Pasquali, L.; Søndergaard, J.N.; Lapins, J.; Nemeth, I.B.; Baltás, E.; Kemény, L.; Homey, B.; Moldovan, L.-I.; Kjems, J.; et al. A comprehensive analysis of coding and non-coding transcriptomic changes in cutaneous squamous cell carcinoma. *Sci. Rep.* **2020**, *10*, 3637. [CrossRef]

84. Wan, J.; Dai, H.; Zhang, X.; Liu, S.; Lin, Y.; Somani, A.K.; Xie, J.; Han, J. Distinct transcriptomic landscapes of cutaneous basal cell carcinomas and squamous cell carcinomas. *Genes Dis.* **2021**, *8*, 181–192. [CrossRef]

85. Brooks, Y.S.; Ostano, P.; Jo, S.H.; Dai, J.; Getsios, S.; Dziunycz, P.; Hofbauer, G.F.; Cerveny, K.; Chiorino, G.; Lefort, K.; et al. Multifactorial ERβ and NOTCH1 control of squamous differentiation and cancer. *J. Clin. Investig.* **2014**, *124*, 2260–2276. [CrossRef] [PubMed]

86. Haider, A.S.; Peters, S.B.; Kaporis, H.; Cardinale, I.; Fei, J.; Ott, J.; Blumenberg, M.; Bowcock, A.M.; Krueger, J.G.; Carucci, J.A. Genomic Analysis Defines a Cancer-Specific Gene Expression Signature for Human Squamous Cell Carcinoma and Distinguishes Malignant Hyperproliferation from Benign Hyperplasia. *J. Investig. Dermatol.* **2006**, *126*, 869–881. [CrossRef]

87. Riker, A.I.; Enkemann, S.A.; Fodstad, O.; Liu, S.; Ren, S.; Morris, C.; Xi, Y.; Howell, P.; Metge, B.; Samant, R.S.; et al. The gene expression profiles of primary and metastatic melanoma yields a transition point of tumor progression and metastasis. *BMC Med. Genom.* **2008**, *1*, 13. [CrossRef]

88. Jee, B.A.; Lim, H.; Kwon, S.M.; Jo, Y.; Park, M.C.; Lee, I.J.; Woo, H.G. Molecular classification of basal cell carcinoma of skin by gene expression profiling. *Mol. Carcinog.* **2015**, *54*, 1605–1612. [CrossRef]

89. Lo, B.K.; Yu, M.; Zloty, D.; Cowan, B.; Shapiro, J.; McElwee, K.J. CXCR3/ligands are significantly involved in the tumorigenesis of basal cell carcinomas. *Am. J. Pathol.* **2010**, *176*, 2435–2446. [CrossRef]

90. Atwood, S.X.; Sarin, K.Y.; Whitson, R.J.; Li, J.R.; Kim, G.; Rezaee, M.; Ally, M.S.; Kim, J.; Yao, C.; Chang, A.L.; et al. Smoothened variants explain the majority of drug resistance in basal cell carcinoma. *Cancer Cell* **2015**, *27*, 342–353. [CrossRef]